

Spin-VCSELs with Local Optical Anisotropies: Toward Terahertz Polarization Modulation

M. Drong^{1,2,3,*}, T. Fördös^{2,3}, H.Y. Jaffrès⁴, J. Peřina Jr.⁵, K. Postava^{2,3}, P. Ciompa^{2,3,4},
J. Piřtora^{2,3} and H.-J. Drouhin¹


¹*LSI, CEA/DRF/IRAMIS, CNRS, École Polytechnique, Institut Polytechnique de Paris, 91120 Palaiseau, France*

²*Nanotechnology Centre, VSB-Technical University of Ostrava, 17. listopadu 2172/15, 708 00 Ostrava-Poruba, Czech Republic*

³*IT4Innovations, VSB-Technical University of Ostrava, 17. listopadu 2172/15, 708 00 Ostrava-Poruba, Czech Republic*

⁴*Unité Mixte de Physique CNRS/Thales and Université Paris-Saclay, 1 Avenue A. Fresnel, 91767 Palaiseau Cedex, France*

⁵*Joint Laboratory of Optics of Palacky University and Institute of Physics of Academy of Sciences of the Czech Republic, Palacky University, 17. listopadu 12, 772 07 Olomouc, Czech Republic*

 (Received 23 June 2020; revised 9 November 2020; accepted 8 December 2020; published 22 January 2021)

We present a semiclassical model for spin-injected vertical-cavity surface-emitting lasers (spin-VCSELs) with local optical anisotropies. Particular focus is put on highly anisotropic spin lasers with broad application potential. A generalized matrix formalism for extraction of the laser modes is introduced, which enables us to calculate the spatial distribution of vectorial modes in arbitrary spin-VCSELs. The time dependence of such laser modes is further studied by means of the generalized coupled-mode theory, which is the natural anisotropic generalization of the conventional mode-decomposition approach. We use the circularly polarized optical modes as the basis for coupled-mode theory, which leads to extension of the well-known spin-flip model. In contrast to the conventional spin-flip model, the only input parameters are the geometric and local optical properties of the multilayer structure and properties of the gain media. The advantages of the theory are demonstrated in the design and optimization of spin-VCSEL structures with a high-contrast grating. We show that the proposed structures can be used for (i) polarization modulation in the terahertz range with tremendous applications for future ultrafast optical communication and (ii) as prospective compact terahertz sources.

DOI: [10.1103/PhysRevApplied.15.014041](https://doi.org/10.1103/PhysRevApplied.15.014041)

I. INTRODUCTION

The fundamental connection of electron and photon spin [1] has led to the development of spin-polarized semiconductor lasers with vertical-cavity surface-emitting laser (VCSEL) geometry [2,3]. In principle, the properties of such devices significantly depend on the degree of spin polarization in their gain media, which involves optical, electrical, or hybrid spin injection [4,5]. Important advances have been achieved in this research field in recent years. For example, it has been shown that VCSELs with spin-polarized gain media exhibit a lower lasing threshold [6,7] and allow direct polarization control [8,9]. Recently, spin amplification using a spin-injected VCSEL (spin-VCSEL) was demonstrated [10]. However, their most-important advantage these days seems to be the possibly ultrafast modulation dynamics, which has the

potential to boost the capacity of optical communication systems [11]. This is possible due to the combination of two factors: an extremely fast spin-mixing rate in the semiconductor quantum wells (QWs) and strong linear optical anisotropies within the VCSEL cavity. It was demonstrated that an In-Al-Ga-As QW VCSEL with modulated spin injection is appropriate for high-speed data communication at telecom wavelength ($\lambda = 1.55 \mu\text{m}$) [12]. More recently, experimental studies using a $\lambda = 850 \text{ nm}$ GaAs QW VCSEL showed that spin modulation can significantly overcome the limitations of conventional VCSELs concerning modulation speed, even by 1 order of magnitude [13]. This is closely related to the possibility of generating coherent terahertz radiation using highly birefringent spin-VCSELs, based on interference of orthogonal linear modes of different frequencies. Such technological improvement would lead to the development of compact tunable terahertz sources operating at room temperatures [14].

*Corresponding author: mariusz.drong@vsb.cz

Concerning steady-state properties, the first qualitative model taking into account both the spin degree of freedom and cavity birefringence was based on the simple Jones-matrix model, discussed more recently in Ref. [15]. It was used to understand basics of polarization dynamics inside spin-VCSELs at the steady state and to interpret the first experimental approaches to quantify and compensate the birefringence [16,17]. A more-extensive formalism has been developed in the framework of 4×4 transfer [18] and the scattering-matrix formalism [19], built upon the ideas in Refs. [20,21]. This layer-by-layer approach has been proven to be able to explain experimental results in great detail, considering local optical properties such as linear and circular anisotropies (i) at the interfaces of III-V semiconductors, (ii) at the surface, and (iii) circular dichroism originating from spin injection into QWs. It is largely useful also for detailed experimental studies of spin-VCSEL anisotropies, as recently shown [22], and eventually for implementing advanced theoretical models of anisotropic QW gain [23–25]. From the perspective of ultrafast dynamics, the integration of spin-VCSELs with highly birefringent photonic crystal mirrors is very promising. The results in Ref. [26] show that the scattering-matrix formalism is one of the most-relevant techniques to model such devices. All of the frameworks mentioned are limited to near-threshold operation. This could eventually be overcome by the above-threshold generalization of the matrix formalism or by using the steady-state-*ab-initio*-lasing-theory algorithm applied to spin-VCSELs [27–29].

On the other hand, the tools for temporal modeling of spin-VCSELs are mainly represented by the spin-flip model (SFM), as the simplified Maxwell-Bloch equations [30,31], derived in a more-intuitive way independently by Travagnin [32], developed originally for conventional VCSELs. The SFM considers the time evolution of circularly polarized field components in the presence of linear birefringence and linear dichroism introduced phenomenologically, ignoring any linear gain anisotropies. Later, also the case of possibly misaligned axes of birefringence and dichroism was considered [33,34], motivated by experimental techniques to induce such phenomena [35]. This was generalized to include the possible frequency variation of QW gain and to explain the polarization switching [36]. A true disadvantage of the SFM is that it cannot describe self-consistently the geometric complexity of the VCSEL cavity and the localized nature of anisotropies, and the dynamics-related parameters must be obtained from experiments. This was solved by robust spatiotemporal models for VCSELs [37,38]. Such models use the shapes of vectorial eigenmodes obtained by solving the cold-cavity problem, taking into account the lateral dimensions of devices and carrier diffusion. More recently, the index-guiding effects and transverse-mode dynamics were studied in Refs. [39,40] using a generalized SFM with anisotropy rates extracted from theory, but for a simple

effective structure. The extensive spatiotemporal modeling of VCSELs is described in an unified way in Refs. [41,42]. Recently, the generalized coupled-mode theory was derived to describe laterally coupled spin-VCSELs [43]; it shares some similarity with our present work. Particular attention should be paid to the laser theory developed originally for coupled-cavity lasers [44], built upon the pioneering work of Haken, Sargent, and Lamb [45,46]. More recently, it was used to describe microcavity lasers, finding excellent agreement with finite-difference time-domain simulations [47]. The approach has been generalized also to describe the lateral effect in half-VCSELs [48,49], but ignoring the detrimental effects of anisotropies and spin pumping.

In this paper, we develop a self-consistent formalism for modeling steady-state and time-dependent emission of spin-VCSELs with large local anisotropies. We generalize the robust matrix formalism, which is based on our previous work [19]. Moreover, we extend the coupled-mode theory of Hodges *et al.* [44]. The model respects the spatial variation of the electric field and its vector nature, together with local anisotropies within the cavity. Additionally, we propose and design spin-VCSEL structures with an intracavity grating. We demonstrate that it is possible to achieve terahertz frequency splitting between modes, which paves the way for important advancements in terahertz photonics.

This paper is organized as follows. In Sec. II, the semi-classical Maxwell-Bloch equations for a spin-VCSEL in the two-level approximation are derived. We consider possible linear anisotropies in the passive cavity as well as inside QWs, in contrast to most approaches to date. In Sec. III, we generalize the matrix formalism. Instead of using active dipolar layers to describe the QW gain, we derive the effective susceptibility of spin-polarized QWs. Consequently, entire structures can be described with use of Yeh's formalism in a unified way. Section IV contains the generalized coupled-mode theory of a spin-VCSEL, derived for circularly polarized vectorial eigenmodes, while the alternative bases are discussed. Our approach allows one to treat self-consistently the entire spin-VCSEL structure, including all local anisotropies, leading, for example, to simple analytic expressions for anisotropy rates. In a certain sense, it can be considered as the time-dependent counterpart to steady-state *ab initio* lasing theory, as noted in Ref. [47]. The theory naturally reduces to an extended SFM, which is derived in Sec. V. The extended SFM describes also the linear gain anisotropy, which is often ignored. Finally, in Sec. VI, we apply the formalism developed to design and optimize the performance of realistic spin-VCSELs with birefringent gratings with large potential for terahertz-photonics applications, such as ultrafast data transfer and generation of coherent terahertz radiation. Appendixes A and B are devoted to the theory of transfer and scattering

matrices and calculation of the cavity decay rate, respectively.

II. SEMICLASSICAL DESCRIPTION OF SPIN-VCSELS

A. General approach and approximations

We now describe the broad picture of how we approach the problem of modeling the lowest-order transverse modes of spin-VCSELS. We use the modified semiclassical spatiotemporal formalism of the Maxwell-Bloch equations, based on a combination of the quantum-mechanical density matrix and Maxwell's classical theory of electrodynamics.

The QW gain medium is modeled by an ensemble of two-level quantum systems distributed inside active layers. Electron conduction-band states (excited) and heavy-hole states in valence band (ground) are coupled via electric dipole interaction, as shown in Fig. 1(a). Each of these levels possesses two spin sublevels, which can be mixed due to relaxation processes. By "spin state," we understand its projection along the z axis. The mixing between heavy-hole spin states can be considered to be much faster than in the case of electrons in the conduction band. The energy difference between excited and ground states near the Γ point $\Delta E = \hbar\omega_0$ is close to the energy of laser-field photons $\hbar\omega$. Thus, any optical coupling to light-hole states is ignored due to heavy-hole–light-hole energy splitting in the QW potential.

We consider only paraxial (with respect to the z axis) wave propagation in the multilayer laser cavity as depicted in Fig. 1(b). In this approximation, the structure is treated layer-by-layer. Thus, our approach is sensitive to any small

changes in the local optical and geometrical properties of any layer, providing a more-realistic description of spin-VCSELS. Optical-material properties of each layer of the structure are described by the permittivity tensor. Such a layer-by-layer strategy for studying spin-VCSELS, with particular focus on optical anisotropies, was demonstrated in our earlier contributions [18,19,22]. Here, we extend our approach to time-domain simulations. We study structures with linear birefringence and linear dichroism in the passive layers, and additionally with linear gain anisotropy inside the active layer, which is often ignored.

B. Optical-material properties

1. Linear birefringence and dichroism inside the cavity

Since our aim is to develop a polarization-sensitive formalism, we briefly mention the typical anisotropies located inside the passive parts of the laser cavity, together with their physical origin. Apart from active-layer anisotropies, which may depend on the gain, spin-VCSEL structures are strongly impacted by the linear birefringence, and the consequent linear dichroism, in the background semiconductor medium. According to detailed theoretical and experimental investigations, this is mostly due to the combined effects of strain in the structures [50] and the phenomena at semiconductor-semiconductor and semiconductor-air interfaces, in which the crystallographic symmetry can be reduced [51]. The strain can be of native origin, caused, for example, by the lattice mismatch of crystal media in neighboring layers, or induced externally by heating or simple mechanical techniques [35]. Another source of anisotropy may be the crystal relaxation in the layer at the top of the VCSEL. Overall anisotropy is enhanced additionally by the electro-optically active media due to the applied static electric field [52].

2. Semiconductor QW with linear gain anisotropy

We now consider the spin-polarized semiconductor QW with linear gain anisotropy. We are particularly interested in the part of the optical response of a semiconductor QW that originates from the pumped-laser transitions in the presence of linear gain anisotropy. In the absence of such anisotropy, radiative electron-hole recombinations in the two spin channels with opposite electron spin projections \uparrow, \downarrow give rise to circularly polarized fields. We use a standard procedure to derive the susceptibility using dipole matrix elements.

We consider the electric dipole approximation, in which the general quantum dipole matrix element is given by [45,53]

$$\theta_{i \rightarrow f} = \int \psi_f^\dagger(\mathbf{r}) \hat{\theta} \psi_i(\mathbf{r}) d^3 \mathbf{r}, \quad (1)$$

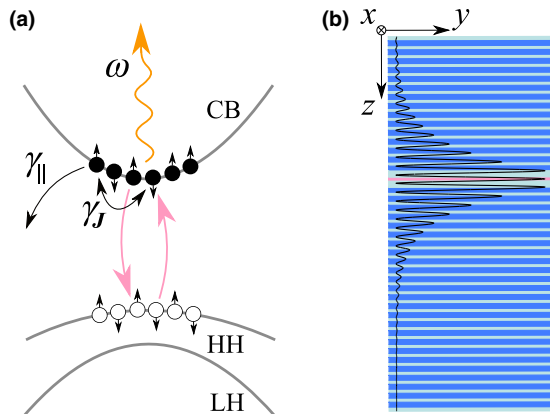


FIG. 1. (a) Approximate band structure inside a semiconductor QW with spin degree of freedom. It is assumed that radiative recombinations occur only between conduction-band (CB) electrons and heavy-hole (HH) states near the Γ point. (b) Spin-VCSEL structure considered here, in which only the propagation of electromagnetic waves parallel to the z axis is considered. LH, light hole.

where $\theta_{i \rightarrow f}$ is the electric-dipole-operator matrix element between states $|i\rangle$ and $|f\rangle$, $\hat{\theta} = [\hat{\theta}_x, \hat{\theta}_y, \hat{\theta}_z]^T$ is the vector of electric dipole operators, and $\psi_i(\mathbf{r})$ and $\psi_f(\mathbf{r})$ are spatial parts of wave functions of coupled initial and final states, respectively.

In the case of a semiconductor QW with quantization axis parallel to z , the dipole matrix elements for two spin channels can be generally written as [24,54]:

$$\begin{aligned}\theta_{\uparrow} &\propto \theta(\mathbf{e}_+ + \beta\mathbf{e}_-), \\ \theta_{\downarrow} &\propto \theta(\mathbf{e}_- + \beta\mathbf{e}_+),\end{aligned}\quad (2)$$

where \mathbf{e}_+ and \mathbf{e}_- are Jones vectors describing the polarization state of circularly polarized optical fields, θ is a certain average dipole matrix element, and β is a general parameter, which describes the linear gain anisotropy under consideration. In the case of a strained QW, with principal axes along the $[110]$ and $[1\bar{1}0]$ crystallographic directions, β can be considered as a band-mixing parameter, which can be determined by *ab initio* calculations [55]. Using such an interpretation, we can write $\beta = -i\mathcal{D}$, where \mathcal{D} is proportional to the difference of applied or internal stress or to equivalent effect along the principal axes: $\sigma_{[110]} - \sigma_{[1\bar{1}0]}$.

Dipole matrix elements of both spin channels $\theta_{\uparrow,\downarrow}$ can be expressed with use of normalized Jones vectors as $\theta_{\uparrow,\downarrow} = \theta \mathbf{e}_{\uparrow,\downarrow}$, which are derived to be

$$\mathbf{e}_{\uparrow} = (\mathbf{e}_{\downarrow})^* = \frac{1}{\sqrt{2(1+\mathcal{D}^2)}} \begin{bmatrix} 1 - i\mathcal{D} \\ -i + \mathcal{D} \end{bmatrix}. \quad (3)$$

The present expression reduces to purely circular eigenmodes (\mathbf{e}_{\pm}) in the absence of any linear anisotropy, giving the standard result obtained with unperturbed electronic wave functions.

Similar results with, however, a different sign convention are obtained with the approach of Fördös *et al.* [19]: by defining the relation between optical transition-matrix elements. Using their mathematical notation, one can introduce linear gain anisotropy in the following way: $\Pi_{[110]} = [1 + (1 - \Delta)/2]\Pi_0$ and $\Pi_{[1\bar{1}0]} = [1 - (1 - \Delta)/2]\Pi_0$, where $\Pi_{[110]}$ and $\Pi_{[1\bar{1}0]}$ stand for transition-matrix elements along anisotropy principal axes and Π_0 is the average matrix element. It can be shown that $\mathcal{D} = (1 - \Delta)/2$.

It appears useful to define the dimensionless susceptibilities $\hat{T}_{\uparrow,\downarrow}$ of particular spin channels using their respective Jones vectors [53]:

$$\hat{T}_{\uparrow,\downarrow} = \mathbf{e}_{\uparrow,\downarrow} \otimes \mathbf{e}_{\uparrow,\downarrow}^{\dagger}. \quad (4)$$

Under pumping, induced-dipole-moment densities $\tilde{\mathbf{P}}_{\uparrow,\downarrow}$ are proportional to $\hat{T}_{\uparrow,\downarrow} \mathbf{E}$ in the steady-state regime.

From now, for simplicity, all of the calculations are performed in the basis spanned by the crystallographic axes $[110]$ and $[1\bar{1}0]$. By this, we mean that the electric field vector will have following components: $\mathbf{E} = [E_{[110]}, E_{[1\bar{1}0]}]^T$. To obtain correct Jones vectors and susceptibilities, one should rotate the reference frame around z by an angle of 45° . Equivalently, we could just take $\beta = \mathcal{D}$. In the given basis, the dimensionless susceptibilities are

$$\hat{T}_{\uparrow} = (\hat{T}_{\downarrow})^* = \frac{1}{2(1+\mathcal{D}^2)} \begin{bmatrix} (1+\mathcal{D})^2 & i(1-\mathcal{D}^2) \\ -i(1-\mathcal{D}^2) & (1-\mathcal{D})^2 \end{bmatrix}. \quad (5)$$

One can see that the dipole interactions of the electromagnetic fields with a specific spin channel are different for waves polarized along the $[110]$ direction or the $[1\bar{1}0]$ direction until $\mathcal{D} = 0$.

C. Maxwell-Bloch equations

Our approach to model the spatiotemporal dynamics of anisotropic spin lasers is based on modified Maxwell-Bloch equations. The modification is based on the fact that we need to describe the anisotropic laser cavity and the gain medium. As already noted, each spin channel in a semiconductor QW is modeled by an ensemble of two-level systems. The time evolution of an open two-level system can be described by a Liouville–von Neumann equation for the density matrix:

$$i\hbar \frac{\partial}{\partial t} \hat{\rho}_{\mu} = [\hat{\mathcal{H}}_{0,\mu} + \hat{\mathcal{H}}_{d,\mu}, \hat{\rho}_{\mu}], \quad (6)$$

where $\mu = \uparrow, \downarrow$. The operator $\hat{\mathcal{H}}_{0,\mu}$ stands for the unperturbed diagonalized Hamiltonian (in the sense of light-matter interaction):

$$\hat{\mathcal{H}}_{0,\mu} = \frac{1}{2} \left[(E_{g,\mu} + E_{e,\mu}) \hat{1} + (E_{g,\mu} - E_{e,\mu}) \hat{\sigma}_z \right], \quad (7)$$

where $E_{g,\mu}$ and $E_{e,\mu}$ are the energies of the ground and excited states at spin channel μ . Operators $\hat{1}$ and $\hat{\sigma}_z$ stand for the unity operator and the diagonal Pauli matrix, respectively.

The ground and excited states are coupled to the electric field via the electric dipole interaction described by the operator

$$\hat{\mathcal{H}}_{d,\mu} = -\hat{\theta}_{\mu} \cdot [\mathbf{E}(\mathbf{r}, t) \exp(i\omega t) + \text{c.c.}], \quad (8)$$

where $\hat{\theta}_{\mu}$ is the electric dipole operator evaluated at the μ th spin channel, \mathbf{E} is the positive-frequency component of the oscillating electric field, and ω is the central frequency of the cavity laser field.

Equations of motion for the density operator are combined with the classical electric field wave equation,

where we assume that the dipole-moment density responsible for the lasing process [defined as $N_{0,\mu} \text{Tr}(\hat{\rho}_\mu \hat{\theta}_\mu) = \tilde{\mathbf{P}}_\mu(\mathbf{r}, t) \exp(i\omega t) + \text{c.c.}$, where $N_{0,\mu}$ is the concentration of idealized two-level systems] represents the source term in the wave equation. We then derive the modified Maxwell-Bloch equations describing the spatiotemporal evolution of the dipole-moment densities $\tilde{\mathbf{P}}_\mu$, spin-carrier concentrations N_μ , and intracavity electric field \mathbf{E} according to [45]

$$\begin{aligned} \frac{\partial}{\partial t} \tilde{\mathbf{P}}_\mu(\mathbf{r}, t) &= -(\gamma_\perp + i\delta_\mu) \tilde{\mathbf{P}}_\mu(\mathbf{r}, t) \\ &+ \frac{i}{\hbar} |\theta|^2 N_\mu(\mathbf{r}, t) \hat{\mathcal{T}}_\mu(\mathbf{r}) \mathbf{E}(\mathbf{r}, t), \end{aligned} \quad (9)$$

$$\begin{aligned} \frac{\partial}{\partial t} N_\mu(\mathbf{r}, t) &= \Lambda_\mu(\mathbf{r}, t) - \gamma_\parallel N_\mu(\mathbf{r}, t) - \gamma_J [N_\mu(\mathbf{r}, t) - N_{\mu'}(\mathbf{r}, t)] \\ &+ \frac{2i}{\hbar} \left[\mathbf{E}^\dagger(\mathbf{r}, t) \tilde{\mathbf{P}}_\mu(\mathbf{r}, t) - \tilde{\mathbf{P}}_\mu^\dagger(\mathbf{r}, t) \mathbf{E}(\mathbf{r}, t) \right], \end{aligned} \quad (10)$$

$$\begin{aligned} &\left[c^2 \nabla^2 - \hat{\epsilon}_m(\mathbf{r}, \omega) \frac{\partial^2}{\partial t^2} - \tilde{\kappa}(\mathbf{r}, \omega) \frac{\partial}{\partial t} \right] \mathbf{E}(\mathbf{r}, t) \exp(i\omega t) \\ &= \frac{1}{\epsilon_0} \frac{\partial^2}{\partial t^2} \sum_{\mu=\uparrow, \downarrow} \tilde{\mathbf{P}}_\mu(\mathbf{r}, t) \exp(i\omega t), \end{aligned} \quad (11)$$

in which all incoherent processes are described phenomenologically by the following quantities: decay rate of density-matrix coherences γ_\perp , spin-carrier pumping rate Λ_μ , decay coefficient γ_\parallel , and spin-mixing rate γ_J . The characteristic decay of the electric field is described by $\tilde{\kappa}$, which is specific for a given design of the optical cavity, and its use is well justified by the Poynting theorem in Appendix B.

Apart from possible gain anisotropies in the QWs, which are described self-consistently by $\hat{\mathcal{T}}_\mu$, it is possible to include any local cavity anisotropies via the relative-permittivity tensor $\hat{\epsilon}_m$ of the background semiconductor medium, which differs from layer to layer.

To provide a complete spatiotemporal solution to these partial differential equations, we chose not to consider any brute-force time-consuming techniques. Instead, we use the transfer-matrix and scattering-matrix formalism to describe the steady-state properties of lasing of spin-VCSELS and the approach based on the coupled-mode theory to investigate the time evolution of optical fields inside spin-VCSELS.

III. STEADY-STATE LASER EMISSION: MATRIX DESCRIPTION

This section introduces an alternative, and more-general, description of multilayer laser structures, such as

spin-VCSELS, based on the transfer-matrix and scattering-matrix formalism, which was first proposed in Ref. [19]. Similarly as here, each layer in the structure was described separately. However, in contrast to our modified approach, active layers required special treatment, since they were approximated as infinitesimally thin active dipolar layers. Such an approximation is not necessary here, which provides several advantages. The use of an active-dipolar-layer approximation is well justified for resonant structures, but the lasing threshold is not determined correctly if one changes the position within the cavity field profile. This is solved self-consistently here. The entire laser structure, together with amplifying active media (QWs or quantum dots), is treated in a straightforward way using the standard Yeh procedure for solving electromagnetic wave propagation inside an arbitrary layered structure [56]. With use of the active-dipolar-layer approximation, the implementation of the formalism for multiple-QW structures becomes difficult. The susceptibility approach is more suitable for incorporating realistic gain spectra of QWs, as well as possible field-saturation effects.

A. Light amplification in spin-polarized anisotropic medium

1. Derivation of susceptibility

For the purposes of the matrix formalism, we derive the electric susceptibility (and later permittivity) of active medium using our modified Maxwell-Bloch equations. Because of the additivity of electric dipole moments, we can write the total dipole-moment density of gain medium as $\mathbf{P} = \mathbf{P}_m + \tilde{\mathbf{P}}$, where \mathbf{P}_m is the background contribution, originating from the optical transitions except the lasing ones, which is given by $\tilde{\mathbf{P}}$. The contribution of lasing transitions in the steady-state operation regime of the laser is

$$\tilde{\mathbf{P}} = \sum_{\mu=\uparrow, \downarrow} \tilde{\mathbf{P}}_\mu = \epsilon_0 \hat{\chi}_a \mathbf{E}, \quad (12)$$

where $\hat{\chi}_a$ stands for the susceptibility of active medium. Assuming $\delta_{\uparrow, \downarrow} = \delta$ and steady-state laser oscillation, Eq. (9) leads to

$$\tilde{\mathbf{P}} = \sum_{\mu=\uparrow, \downarrow} i \frac{1}{\gamma_\perp + i\delta} \frac{|\theta|^2}{\hbar} N_\mu \hat{\mathcal{T}}_\mu \mathbf{E}. \quad (13)$$

Comparing this result with Eq. (12), we can derive

$$\hat{\chi}_a = i \frac{1}{\gamma_\perp + i\delta} \frac{|\theta|^2}{\hbar \epsilon_0} \left(N_\uparrow \hat{\mathcal{T}}_\uparrow + N_\downarrow \hat{\mathcal{T}}_\downarrow \right). \quad (14)$$

Because we know that the optical response of a QW is not described by a Lorentz line shape, we use the approximate relation between frequency detuning δ and

the inverse coherence lifetime γ_{\perp} : $\alpha = \delta/\gamma_{\perp}$, where α is the linewidth enhancement factor. Additionally, the steady-state values of spin-carrier concentrations $N_{\uparrow,\downarrow}$ can be straightforwardly calculated with Eq. (10). $N_{\uparrow,\downarrow}$ are generally functions of the electric field, which leads to a nonlinear problem. However, this is beyond the scope of the present work, since we are interested mainly in the near-threshold steady-state oscillation. Consequently, the expression for the susceptibility contribution responsible for light amplification $\hat{\chi}_a$ can be written in a compact form as

$$\hat{\chi}_a = i\bar{\chi}(1 - i\alpha)\hat{T}, \quad (15)$$

where the definition of the optical gain tensor \hat{T} from Ref. [19] ($N_{\uparrow} + N_{\downarrow}$) $\hat{T} = N_{\uparrow}\hat{T}_{\uparrow} + N_{\downarrow}\hat{T}_{\downarrow}$ is used:

$$\hat{T} = \frac{1}{2(1 + \mathcal{D}^2)} \begin{bmatrix} (1 + \mathcal{D}^2) & i(1 - \mathcal{D}^2)\mathcal{P}_s \\ -i(1 - \mathcal{D}^2)\mathcal{P}_s & (1 - \mathcal{D}^2)^2 \end{bmatrix}, \quad (16)$$

in which the effective degree of electron spin polarization \mathcal{P}_s is introduced. According to Eq. (10), when $\mathbf{E} \rightarrow 0$ (at the threshold), we can write

$$\mathcal{P}_s = \frac{\gamma_{\parallel}}{\gamma_{\parallel} + 2\gamma_J} \mathcal{P}_J, \quad (17)$$

where \mathcal{P}_J is the pump spin polarization. The fact that pumping rates $\Lambda_{\uparrow,\downarrow}$ can be expressed using unsaturated carrier concentrations $N_{0\uparrow,\downarrow}$ is used. The scalar part $\bar{\chi}$ is defined as

$$\bar{\chi} = \frac{1}{(1 + \alpha^2)\gamma_{\perp}} \frac{|\theta|^2}{\hbar\epsilon_0} (N_{0\uparrow} + N_{0\downarrow}). \quad (18)$$

The specific line shape (Lorentz in this case) is not considered, because $\bar{\chi}$ is controlled quantity here as a certain normalized pump rate, or the quantity to be found in the case of the threshold condition. In this way, we model a relatively broad gain profile of a semiconductor QW. This can be further generalized to describe more precisely the dependence on carrier concentration and photon frequency by going beyond the approximation for two-level gain medium.

The total electric susceptibility consists of a background part $\hat{\chi}_m$ and an active part $\hat{\chi}_a$, which is generally time dependent due to carrier dynamics:

$$\hat{\chi}(\mathbf{r}, \omega, t) = \hat{\chi}_m(\mathbf{r}, \omega) + \hat{\chi}_a(\mathbf{r}, \omega, t). \quad (19)$$

As one can expect, this time dependence is ignored in the present section.

2. Wave equation in the active medium

To derive the total matrix of the system we are considering, we solve the wave equation in each layer separately. Since most of the layers in the laser system are optically isotropic or have weak anisotropies, we are primarily interested in solving the wave equation in the active layers. The propagation constants and polarization eigenmodes are derived.

The wave equation (11) reduces in the steady state to

$$\left[c^2 \nabla^2 - \hat{\epsilon}(\mathbf{r}, \omega) \frac{\partial^2}{\partial t^2} \right] \mathbf{E}(\mathbf{r}) \exp(i\omega t) = 0, \quad (20)$$

where we assume that any decay processes in the cavity described by $\tilde{\kappa}$ are self-consistently included by the transfer-matrix formalism. We introduce the total-relative-permittivity tensor $\hat{\epsilon}(\mathbf{r}, \omega) = \hat{1} + \hat{\chi}_m(\mathbf{r}, \omega) + \hat{\chi}_a(\mathbf{r}, \omega)$. The spatial variation of the field inside the active layer can be described by plane waves: $\mathbf{E}(\mathbf{r}) = \mathbf{E}_0 \exp(-i\mathbf{q}\mathbf{r})$, where \mathbf{E}_0 is the amplitude of the electric field inside the active layer. We know that, differential operators from the wave equation act as follows: $\nabla \rightarrow -i\mathbf{q}$ and $\partial_t \rightarrow i\omega$. Omitting the spatial variation of permittivity, since we analyze a single layer, we obtain the Helmholtz equation:

$$\left[\hat{\epsilon} \left(\frac{\omega}{c} \right)^2 - \mathbf{q}^2 \right] \mathbf{E}_0 = 0. \quad (21)$$

Two assumptions are used here. First, only the propagation parallel to z is considered, so the normalized propagation constant is defined as $\tilde{q} = |\mathbf{q}|/(\omega/c)$, which stands for z component of the wave vector normalized to the vacuum wave number. Second, we use the isotropic background medium $\hat{\epsilon}_m = \epsilon_{\text{QW}}\hat{1}$. The possible generalization for anisotropic background semiconductor media is straightforward and does not create any difficulty. Using Eqs. (15) and (21), and approximating the term $1/[2(1 + \mathcal{D}^2)]$ using $1/2$, since \mathcal{D}^2 is typically very small ($\mathcal{D}^2 \ll 1$), we derive the normalized propagation constants inside the active layers:

$$\begin{aligned} \tilde{q}_{1,2}^2 &= \epsilon_{\text{QW}} + i\frac{\bar{\chi}}{2}(1 - i\alpha)(1 + \mathcal{D}^2) \\ &\pm i\frac{\bar{\chi}}{2}(1 - i\alpha)\sqrt{(2\mathcal{D})^2 + [(1 - \mathcal{D}^2)\mathcal{P}_s]^2}. \end{aligned} \quad (22)$$

Because of anisotropies, this result contains four possible propagation constants, describing two forward-propagating waves and two backward-propagating waves, which build up the resulting standing wave.

3. Phase-amplitude coupling

Although the anisotropy parameter \mathcal{D} is introduced to quantify the linear gain anisotropy, its nonzero value has

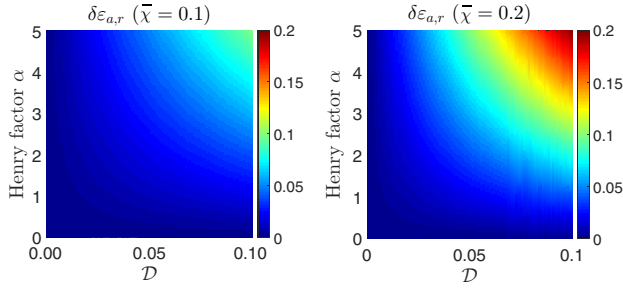


FIG. 2. Birefringence $\delta\epsilon_{a,r}$ induced by phase-amplitude coupling as a function of the gain dichroism \mathcal{D} and the Henry factor α .

consequences for phase anisotropies. It is well known that due to phase-amplitude-coupling mechanisms the gain anisotropy may contribute to the birefringence of the medium. We assume, for example, a strained quantum well with $\mathcal{P}_s = 0$. In our convention, the permittivity tensor of such medium would be diagonal with different values for waves polarized along the $[110]$ and $[1\bar{1}0]$ directions:

$$\begin{aligned}\epsilon_{a,xx} &= \epsilon_{\text{QW}} + i \frac{\bar{\chi}}{2} (1 - i\alpha)(1 + \mathcal{D})^2, \\ \epsilon_{a,yy} &= \epsilon_{\text{QW}} + i \frac{\bar{\chi}}{2} (1 - i\alpha)(1 - \mathcal{D})^2.\end{aligned}\quad (23)$$

Induced linear birefringence can be quantified using the difference of real parts of ϵ_{xx} and ϵ_{yy} . The calculation yields

$$\delta\epsilon_{a,r} = \text{Re}\{\epsilon_{a,xx} - \epsilon_{a,yy}\} = 2\bar{\chi}\alpha\mathcal{D}. \quad (24)$$

Assuming typical values $\bar{\chi} = 0.1$, $\alpha = 3$, and $\mathcal{D} = 0.025$ (or equivalently $1 - \Delta \cong 0.95$, as extracted from experimental data in Ref. [19]), one obtains $\delta\epsilon_{a,r} = 0.015$. In the case of a monolithic VCSEL, it can induce frequency splitting of several gigahertz. With $\alpha = 0$ there is no effective birefringence due to linear gain anisotropy, as shown in Fig. 2.

B. The resonance condition

The threshold modes of the spin-VCSEL structure are used in Sec. IV as a basis for the time-dependent coupled-mode theory. The exact spatial distribution of threshold modes is used to evaluate overlap integrals, which describe effects of perturbations in the optical cavity, such as optical anisotropies. In the following, the procedure to extract such modes is described.

The eigenmode extraction is demonstrated for a model multiple-QW structure as depicted in Fig. 3. According to Appendix A, the characteristic matrix of the general n th layer is $\mathbf{T}^{(n)} = \mathbf{D}^{(n)}\mathbf{P}^{(n)}[\mathbf{D}^{(n)}]^{-1}$, where $\mathbf{D}^{(n)}$ is a dynamic matrix, which is used to calculate the components of the electromagnetic field using amplitudes of particular running waves. The propagation and the amplification of

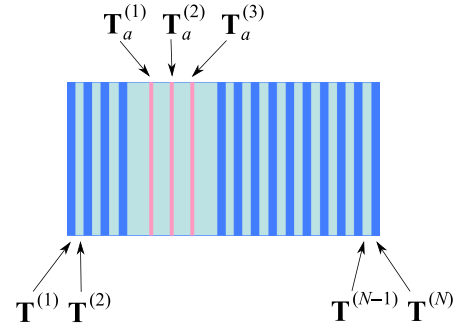


FIG. 3. A multiple-QW spin-VCSEL device consisting of $N + 3$ layers. Each layer is described by its own permittivity tensor $\hat{\epsilon}^{(n)}$ and thickness $d^{(n)}$.

running waves in the medium is given by $\mathbf{P}^{(n)}$. The notation $\mathbf{T}_a^{(n)}$ stands for the characteristic matrix of the n th active layer. According to Eq. (A6), the total matrix \mathbf{M} is given by

$$\mathbf{M} = [\mathbf{D}^{(0)}]^{-1} \mathbf{T}^{(1)} \dots \mathbf{T}_a^{(1)} \dots \mathbf{T}^{(N)} \mathbf{D}^{(N+1)}. \quad (25)$$

$\mathbf{M} = \mathbf{M}(\lambda, \bar{\chi})$, where the wavelength λ and the scalar part of the active-layer susceptibility $\bar{\chi}$, which is proportional to the pump rate, are the quantities to be found. Their threshold values can be found by satisfying the waveguiding condition:

$$\mathbf{M}_{11}\mathbf{M}_{33} - \mathbf{M}_{13}\mathbf{M}_{31} = 0. \quad (26)$$

Alternatively, the scattering matrix \mathbf{S} of the system can be calculated, allowing a more-straightforward calculation of the amplitudes \mathbf{A}_{out} of emitted waves:

$$\mathbf{S}^{-1}\mathbf{A}_{\text{out}} = 0. \quad (27)$$

One can see that the condition for a nontrivial solution is

$$\det(\mathbf{S}^{-1}) = [\det(\mathbf{S})]^{-1} = 0, \quad (28)$$

which is equivalent to the standard waveguiding condition in the transfer-matrix formalism [see Eq. (26)].

IV. TEMPORAL COUPLED-MODE THEORY

A. The basis

1. The basis of circularly polarized fields

In this section, we develop and describe the coupled-mode theory of spin-VCSELS based on the Maxwell-Bloch equations derived in Sec. II C. We adopt and generalize the approach first introduced in Ref. [44] and more recently in Ref. [47]. Consequently, our derivations are structured according to these studies. The approach is based on the projection of the Maxwell-Bloch equations onto a certain

basis, which is specific for each cavity; in particular, the vector nature of the basis functions is respected. Additionally, our basis functions are calculated for the active device, in contrast to most studies [37,40]. It allows one to include self-consistently all of the polarization-dependent properties of the cavity.

There are more possible options for choosing a correct basis, which are discussed later. In this work, we derive the coupled-mode equations using the basis of circularly polarized fields, which can be obtained from our modified matrix approach for the extraction of the laser eigenmodes. We comment on several reasons, which are mostly practical, why such a basis is the appropriate one: (i) The first reason lies in the optical selection rules and in the fact that particular radiative electron-hole recombinations in a device of spin-VCSEL geometry generate circularly polarized photons. In this sense, the anisotropies within the cavity can be considered as perturbations of those circular basis functions. (ii) The second reason for using the circular basis is because of its mathematical properties. We know that the positive-frequency component of the electric field can be generally decomposed into

$$|E\rangle = \sum_k E_k |k\rangle \exp(i\delta\omega_k t), \quad (29)$$

where we use the compact bra-ket notation to avoid the tedious integral equations in the next parts of this paper. E_k stands for the time-dependent amplitude of eigenmode (or basis function, alternatively) $|k\rangle$ and $\delta\omega_k$ is the frequency shift of a given mode with respect to a certain central frequency ω (see Sec. II C) of laser-field oscillations. The circular basis can be considered as degenerate from the frequency point of view and thus $\delta\omega_k \rightarrow 0$. In this case the total field can be decomposed as a sum $|E\rangle = E_+ |+\rangle + E_- |-\rangle$, which significantly simplifies the mathematical derivations. The next practical advantage is the orthogonality of circular basis $\langle + | - \rangle = 0$. (iii) The last reason is that we wish to show the connection to some previous work in this field. Namely, to provide a rigorous background to the well-known SFM as well as its extension.

Typical shapes of the basis functions $\varphi_{\pm}(z) = \langle z | \pm \rangle$ calculated numerically are shown in Fig. 4 as a function of position within the cavity.

2. Other basis options

Generally, the choice of a particular basis depends on the properties of the laser structure. For example, in our polarization-focused approach, one can estimate which element of the laser cavity (such as spin-polarized QWs, or birefringent layers in Bragg reflectors) is the most dominant in determining the laser's performance.

Consequently, in the case of a structure with very strong optical anisotropies, such as strained VCSELs studied in

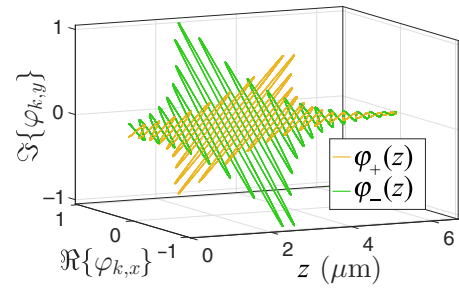


FIG. 4. The spatial distribution of the basis functions $\varphi_k(z) = \langle z | k \rangle$ within the laser cavity.

Ref. [13], it would be more appropriate to choose linearly polarized basis functions. There are two options for how to apply the linear basis. First, one can use orthogonal linear functions with degenerate frequencies. Any anisotropies, such as the linear birefringence or the gain anisotropy originating from electron spin imbalance in active regions, play the role of perturbations. Another option is to use linear basis functions of different frequency, calculated using an already-anisotropic laser cavity. Although this leads to mathematical difficulties, such an approach is very useful for analysis of lasers with photonic crystals or gratings, which are studied in Sec. VI.

Alternatively, it is possible to construct the coupled-mode theory for the real eigenmodes, which do not have to be orthogonal. The ansatz for the electric field looks slightly different in this case (the idea is based on the work in Ref. [43]):

$$\mathbf{E}(z, t) = \sum_k \mathbf{E}_k(t) \varphi_k(z) \exp(i\delta\omega_k t).$$

We use standard notation here to emphasize that in this case the time-dependent amplitudes \mathbf{E}_k contain the polarization vector and we consider only scalar spatially varying basis functions φ_k . The approximation here is that φ_k is time independent, which introduces only a small inaccuracy in the formalism.

B. Derivation of the coupled-mode equations

1. Dipole-moment-density decomposition

The first step in deriving the rate equations consists in expressing the dipole-moment density $\tilde{\mathbf{P}}$ in the circular basis considered. We use the compact bra-ket notation, and thus Eq. (9) becomes

$$\frac{\partial}{\partial t} |\tilde{P}_\mu\rangle = -(\gamma_\perp + i\delta) |\tilde{P}_\mu\rangle + i \frac{|\theta|^2}{\hbar} N_\mu \hat{T}_\mu |E\rangle. \quad (30)$$

Dipole-moment densities and the electric field are now expanded using the same basis functions $\{|+\rangle, |-\rangle\}$. We

make the following projection ansatz for each of them:

$$\begin{aligned} |\tilde{P}_\mu\rangle &= \sum_{k=+,-} \tilde{P}_{\mu,k} |k\rangle, \\ |E\rangle &= \sum_{k=+,-} E_k |k\rangle, \end{aligned} \quad (31)$$

where $|k\rangle = \mathbf{e}_k|\varphi\rangle$ can be separated into a polarization part \mathbf{e}_k and a spatial part $|\varphi\rangle$ in the case of a given basis. Inserting the ansatz for Eq. (30) and multiplying using $\langle j|\varepsilon_m$ from the left, we obtain

$$\begin{aligned} \frac{\partial}{\partial t} \sum_k \langle j|\varepsilon_m|k\rangle \tilde{P}_{\mu,k} &= -(\gamma_\perp + i\delta) \sum_k \langle j|\varepsilon_m|k\rangle \tilde{P}_{\mu,k} \\ &+ i \frac{|\theta|^2}{\hbar} \sum_k \langle j|\varepsilon_m N_\mu \hat{T}_\mu |k\rangle E_k. \end{aligned} \quad (32)$$

Acting using $\langle j|\varepsilon_m$ is mathematically equivalent to constructing the variational formulation, similarly to the framework of finite-element methods. $\varepsilon_m = \varepsilon_m(z)$ stands for the isotropic part of the background permittivity in the sense of $\hat{\varepsilon}_m = \varepsilon_m \hat{1} + \delta \varepsilon_m$. On the basis of the properties of basis chosen, we evaluate scalar products as $\langle j|\varepsilon_m|k\rangle = \mathbf{e}_j^\dagger \mathbf{e}_k (\varphi|\varepsilon_m|\varphi) = \delta_{jk} \mathcal{I} = \delta_{jk} \int_C \varepsilon_m(z) |\varphi(z)|^2 dz$. Using this result, we derive

$$\begin{aligned} \frac{d}{dt} \tilde{P}_{\mu,j} &= -(\gamma_\perp + i\delta) \tilde{P}_{\mu,j} \\ &+ i \frac{|\theta|^2}{\hbar} \mathcal{I}^{-1} \sum_k \mathcal{N}_\mu g_\mu^{jk} E_k. \end{aligned} \quad (33)$$

The optical gain is polarization dependent, which is included in the coefficient $g_\mu^{jk} = \mathbf{e}_j^\dagger \hat{T}_\mu \mathbf{e}_k$, where \mathbf{e}_j and \mathbf{e}_k are the Jones vectors describing the polarization state of the basis functions. It is necessary to introduce the time-dependent quantity \mathcal{N}_μ , defined as

$$\mathcal{N}_\mu = (\varphi|\varepsilon_m N_\mu|\varphi). \quad (34)$$

Mathematically, this represents the overlap integral of the spin-carrier concentration.

Since class-C lasers are not considered in the present work, we assume that the dipole-moment density follows the electric field adiabatically by taking $\partial_t \tilde{P}_{\mu,j} = 0$. Additionally, it can be shown that the total laser dipole-moment density can be decomposed in the circular basis as

$$|\tilde{P}\rangle = \sum_k \underbrace{(\tilde{P}_{\uparrow,k} + \tilde{P}_{\downarrow,k})}_{\tilde{P}_k} |k\rangle. \quad (35)$$

Consequently, Eq. (33) leads to

$$\tilde{P}_j = i \frac{1}{\gamma_\perp + i\delta} \frac{|\theta|^2}{\hbar} \mathcal{I}^{-1} \sum_{\mu=\uparrow,\downarrow} \sum_{k=+,-} \mathcal{N}_\mu g_\mu^{jk} E_k, \quad (36)$$

which is the adiabatic reformulation of Eq. (9) in the given basis and where we define $g_\mu^{jk} = \mathbf{e}_j^\dagger \hat{T}_\mu \mathbf{e}_k$. The interpretation of Eq. (36) is as follows: Generally, in the presence of a linear gain anisotropy inside the active layers, circularly polarized fields are coupled to each other. One particular circularly-polarized-field component induces not only its own dipole-moment density but also a small amount of the orthogonal one due to off-diagonal coefficients g_μ^{jk} .

2. Photons

The derivation of the equations of motion describing the time evolution of the electric field within the spin-VCSEL cavity is based on Eq. (11), to which the slowly-varying-envelope approximation is applied to get rid of second-order time derivatives. The same strategy as in the case of the dipole-moment density is used for the derivation of field coupled-mode equations. Namely, we express the wave equation in bra-ket notation and then we project electric field and dipole moment density onto the chosen basis. Thus, we have

$$\begin{aligned} \frac{\partial}{\partial t} |E\rangle &= -i \frac{\omega}{2\varepsilon_{\text{QW}}} |\tilde{P}\rangle \\ &- \left(\frac{\tilde{\kappa}}{2} + i \frac{\omega}{2} + i \frac{c^2}{2\omega} \hat{\varepsilon}_m^{-1} \frac{\partial^2}{\partial z^2} \right) |E\rangle, \end{aligned} \quad (37)$$

where it is assumed that the active-medium background is described by its permittivity ε_{QW} . Otherwise, the remaining part of the cavity is described generally by its permittivity tensor $\hat{\varepsilon}_m$ in order to describe self-consistently any anisotropies. It is useful to define the so-called anisotropy operator $\hat{\gamma}$:

$$\hat{\gamma} = i \frac{\omega}{2} + i \frac{c^2}{2\omega} \hat{\varepsilon}_m^{-1} \frac{\partial^2}{\partial z^2}. \quad (38)$$

As shown later, the well-known anisotropy rates used in the spin-flip model, such as γ_p and γ_a , can be calculated from normalized off-diagonal matrix elements of $\hat{\gamma}$.

Using Eq. (31) and multiplying the wave equation from the left, using $\langle j|\varepsilon_m$, one obtains

$$\begin{aligned} \frac{\partial}{\partial t} \sum_k \langle j|\varepsilon_m|k\rangle E_k &= -i \frac{\omega}{2\varepsilon_{\text{QW}}} \sum_k \langle j|\varepsilon_m|k\rangle \tilde{P}_k \\ &- \frac{1}{2} \sum_k \langle j|\varepsilon_m \tilde{\kappa} |k\rangle E_k \\ &- \sum_k \langle j|\varepsilon_m \hat{\gamma} |k\rangle E_k. \end{aligned} \quad (39)$$

Because of the orthogonality of the circular basis, we know that $\langle j | \varepsilon_m | k \rangle = \delta_{jk} \mathcal{I}$. We use the notation $\gamma_{jk} = \langle j | \varepsilon_m \hat{\gamma} | k \rangle$ for anisotropy-operator matrix elements. Next we introduce the gain coefficient \mathcal{G} defined as $\mathcal{G}(\omega) = |\theta|^2 \omega / 2\hbar \varepsilon_{\text{QW}} (1 + \alpha^2) \gamma_{\perp}$, where $\alpha = \delta / \gamma_{\perp}$ stands for the linewidth enhancement factor [57]. Finally, using the expression for \tilde{P}_j from Eq. (36), we derive the general rate equation for the field amplitude E_j :

$$\begin{aligned} \frac{d}{dt} E_j &= \mathcal{G}(\omega) (1 - i\alpha) \mathcal{I}^{-1} \sum_{\mu=\uparrow,\downarrow} \sum_{k=+,-} \mathcal{N}_{\mu} g_{\mu}^{jk} E_k \\ &\quad - \kappa E_j - \mathcal{I}^{-1} \sum_{k=+,-} \gamma_{jk} E_k, \end{aligned} \quad (40)$$

where the cavity decay rate

$$\kappa = \frac{1}{2} \frac{\langle j | \varepsilon_m \tilde{\kappa} | j \rangle}{\langle j | \varepsilon_m | j \rangle} \quad (41)$$

is defined. Equation (40) involves self-consistently the anisotropic character of the structure, not only of the passive cavity background but also of the gain medium itself. Moreover, it is sensitive to any small changes in the geometry of spin-VCSEL structures.

3. Spin carriers

We now turn to the dynamics of the spin-polarized carriers coupled to the electromagnetic field. We derive the rate equations for the overlaps \mathcal{N}_{μ} , as suggested by Eq. (33).

Equation (10) may be expressed with bra-ket notation as

$$\begin{aligned} \frac{\partial}{\partial t} N_{\mu} &= \Lambda_{\mu} - \gamma_{\parallel} N_{\mu} - \gamma_J (N_{\mu} - N_{\mu'}) \\ &\quad + \frac{2i}{\hbar} \left(\langle E | \delta_{zz'} | \tilde{P}_{\mu} \rangle - \text{c.c.} \right), \end{aligned} \quad (42)$$

where we use the filtration property of the Dirac δ function $\delta_{zz'} = \delta(z - z')$.

To transform N_{μ} into \mathcal{N}_{μ} , we act using $(\varphi | \varepsilon_m (\dots) | \varphi)$ on both sides of Eq. (42), in which we use Eq. (31). We obtain

$$\begin{aligned} \frac{d}{dt} \mathcal{N}_{\mu} &= -\gamma_{\parallel} (\mathcal{N}_{\mu} - \mathcal{N}_{0\mu}) - \gamma_J (\mathcal{N}_{\mu} - \mathcal{N}_{\mu'}) \\ &\quad + \frac{2i}{\hbar} \mathcal{W} \sum_k (E_k^* \tilde{P}_{\mu,k} - \text{c.c.}), \end{aligned} \quad (43)$$

where we use the relation $\Lambda_{\mu} = \gamma_{\parallel} N_{0\mu}$ and where the coupling coefficients \mathcal{W} are identified as the spatial overlap of the basis functions over the active region according to

$$\mathcal{W} = (\varphi | \varepsilon_m (\varphi | \delta_{zz'} | \varphi) | \varphi) = \int_a \varepsilon_m(z') |\varphi(z')|^4 dz'. \quad (44)$$

They describe how the generalized optical intensities $E_k^* E_l$ interact with spin-carrier overlaps, respecting the spatial

distribution of modes as well as the polarization-dependent gain.

After having inserted $\tilde{P}_{\mu,k}$, which is adiabatically eliminated in Eq. (33), one obtains

$$\begin{aligned} \frac{d}{dt} \mathcal{N}_{\mu} &= -\gamma_{\parallel} (\mathcal{N}_{\mu} - \mathcal{N}_{0\mu}) - \gamma_J (\mathcal{N}_{\mu} - \mathcal{N}_{\mu'}) \\ &\quad - \tilde{\mathcal{G}} \mathcal{I}^{-1} \mathcal{W} \sum_{k=+,-} \sum_{l=+,-} \text{Re}\{g_{\mu}^{kl} E_k^* E_l\} \mathcal{N}_{\mu}, \end{aligned} \quad (45)$$

where the coupling coefficient $\tilde{\mathcal{G}} = 4|\theta|^2 / \hbar^2 (1 + \alpha^2) \gamma_{\perp}$ is defined.

Equations (40) and (45) form the general framework for our time-dependent modeling of spin-VCSEL structures of any variation of cavity parameters and optical properties, such as local anisotropies along the z axis. They consist of two equations of motion for the field amplitudes E_j corresponding to the two different modes, and two differential equations for spin-carrier spatial overlaps \mathcal{N}_{μ} .

4. Discussion: spatially varying gain properties

In the most-general cases, it is necessary to find equations of motion (eight in total) for spin-carrier overlaps \mathcal{N}_{μ}^{jk} defined as

$$\mathcal{N}_{\mu}^{jk} = \langle j | \varepsilon_m N_{\mu} \hat{T}_{\mu} | k \rangle, \quad (46)$$

which appear in Eq. (32). Such a definition respects the polarization-dependent optical response of the laser transitions. Thus, it is a natural generalization of the population overlap integrals $\mathcal{N}^{jk} = \langle j | \varepsilon_m N | k \rangle$ used in Refs. [44,47].

Overlap integrals \mathcal{N}_{μ}^{jk} defined in such a way are very important for devices in which the optical properties of QWs depend on the position. For example, the strain field does not have to be uniform everywhere, resulting in different values of gain anisotropy \mathcal{D} across the laser cavity.

Only two of them ($\mathcal{N}_{\uparrow}^{++}$ and $\mathcal{N}_{\downarrow}^{--}$) would be nonzero in the absence of any linear gain anisotropy ($\mathcal{D} \rightarrow 0$).

C. Theory of anisotropy rates

The important advantage of our coupled-mode theory is that the entire optical cavity is treated in a unified way and all perturbations, such as anisotropies, are introduced by the overlap integrals. Equivalently, one can say that anisotropy rates can be calculated using the matrix elements of the anisotropy operator $\hat{\gamma}$, which is derived from the Maxwell-Bloch equations. Qualitatively, very similar approach can be found in Ref. [58], dealing with the theory of a Zeeman laser. We now express the general matrix

element γ_{jk} in the familiar integral notation according to

$$\begin{aligned} \gamma_{jk} &= \langle j | \varepsilon_m \hat{\gamma} | k \rangle \\ &= \int_C \boldsymbol{\varphi}_j^\dagger \varepsilon_m \left(i \frac{\omega}{2} + i \frac{c^2}{2\omega} \hat{\varepsilon}_m^{-1} \frac{\partial^2}{\partial z^2} \right) \boldsymbol{\varphi}_k dz, \end{aligned} \quad (47)$$

where the integration is performed over the entire cavity. One can observe that different behavior can be expected from the diagonal and off-diagonal anisotropy coupling constants, because the first term under the integral will disappear when $j \neq k$. It can be shown that diagonal matrix elements γ_{jj} lead to equal frequency shifts of both laser modes in the same direction on the frequency axis. This statement applies for structures with permittivity tensors containing ‘‘usual’’ anisotropies such as linear birefringence. From now on, we do not consider the diagonal contributions and we omit the first term of $\hat{\gamma}$.

In practice, the terms $\tilde{\gamma}_{jk} = \mathcal{I}^{-1} \gamma_{jk}$ have the physical meaning of anisotropy rates. We can separate the basis functions into polarization and scalar (spatial) components as $\boldsymbol{\varphi}_j = \mathbf{e}_j \varphi$. Using Eq. (47), one gets

$$\tilde{\gamma}_{jk} = i \frac{c^2}{2\omega} \sum_n \frac{\varepsilon_n \int_n \varphi^* (\partial_{zz}^2 \varphi) dz}{\int_C \varepsilon_m |\varphi|^2 dz} \left[\mathbf{e}_j^\dagger (\hat{\varepsilon}_n^{-1}) \mathbf{e}_k \right], \quad (48)$$

where the integration over the entire cavity is replaced by the summation of contributions of anisotropic layers indexed by n . Contributions of isotropic layers are equal to zero, as can be expected. The permittivity tensor in the n th layer is noted as $\hat{\varepsilon}_n$. The expression obtained for $\tilde{\gamma}_{jk}$ can be further simplified by describing the shape of φ in the n th layer by the superposition of respective forward-propagating and backward-propagating planar waves of respective amplitudes F_n and B_n : $\varphi(z) = F_n e^{-iq_n(z-z_n)} + B_n e^{iq_n(z-z_n)}$, where z_n is the position of the $(n-1/n)$ interface. The wave number q_n can be written as $q_n^2 = \varepsilon_n(\omega/c)^2$, where ε_n is the isotropic part of the permittivity tensor. Finally, the expression for $\tilde{\gamma}_{jk}$ reads

$$\tilde{\gamma}_{jk} = -i \frac{\omega}{2} \sum_n \Gamma_n \left[\mathbf{e}_j^\dagger (\hat{\varepsilon}_n^{-1}) \mathbf{e}_k \right] \varepsilon_n, \quad (49)$$

where Γ_n is the optical confinement factor of the n th anisotropic layer. The minus sign originates here from the second-order derivative of φ . As we show later, this expression contains the well-known birefringence and dichroism rates of the conventional spin-flip model. Moreover, the approach allows one to derive anisotropy rates for arbitrary anisotropy, especially in structures containing more-exotic anisotropies. Some of the examples include devices with optical metasurfaces or devices with non-collinear axes of anisotropies.

V. EXTENDED SPIN-FLIP MODEL

We now describe in detail the connection between our theoretical perturbative framework and the SFM and show that our method may generalize the previous simplified approach.

A. Well-designed structures

1. Simplifying assumptions

In most cases, active layers are generally located in the antinodes of the oscillating electromagnetic field standing wave. Additionally, we may assume that each active layer within the cavity, such as a QW, is homogeneously excited by the same polarized field, and the polarization state of the optical field does not change significantly from point to point between active layers. In this case, it does not create any difficulty to guess an approximate function that describes the spatial variation of spin carriers inside a QW laser, assuming that radiative recombination occurs only in the volume of a QW.

For that reason, we write the spin-carrier populations as

$$N_{\uparrow,\downarrow}(z, t) = n_{\uparrow,\downarrow}(t) \phi(z), \quad (50)$$

where ϕ is the typical function one considers to describe the spatial distribution of spin carriers and $n_{\uparrow,\downarrow}$ are the time-dependent spin-carrier concentrations. We choose to use a set of simple rectangular functions. This may appear to be a very strong approximation but is well justified by the fact that the electronic wave functions inside the QW are strongly localized. The function ϕ has the following properties:

$$\begin{aligned} \phi(z) &= 1, & z \in \{a\}, \\ \phi(z) &= 0, & z \in \{C\} \setminus \{a\}, \end{aligned} \quad (51)$$

where $\{a\}$ and $\{C\}$ are the sets of all points inside the active layer and the entire optical cavity, respectively, in this one-dimensional approximation. Assuming such a spatial distribution of spin carriers, their overlaps become $\mathcal{N}_\mu = n_\mu (\varphi | \varepsilon_m | \varphi)_a$, where $(\varphi | \varepsilon_m | \varphi)_a = \int_a \varepsilon_m(z) |\varphi(z)|^2 dz$. As follows from the definition of ϕ , the integration is performed over the active region. Moreover, it can be shown that $\mathcal{I}^{-1} \mathcal{N}_\mu = \Gamma n_\mu$, where

$$\Gamma = \frac{\int_a \varepsilon_m(z) |\varphi(z)|^2 dz}{\int_C \varepsilon_m(z) |\varphi(z)|^2 dz} \quad (52)$$

represents the conventional optical confinement factor, quantifying the relative amount of electromagnetic field energy confined in the active region.

2. Reduced rate equations

Applying all the above-mentioned arguments to Eqs. (40) and (45), we simplify the description of spin-laser

structures. Namely, we get rid of not-intuitively-defined quantities $\mathcal{N}_{\uparrow,\downarrow}$. The resulting rate equations are

$$\begin{aligned} \frac{d}{dt}E_j &= \mathcal{G}(\omega)(1 - i\alpha)\Gamma \sum_{\mu=\uparrow,\downarrow} \sum_{k=+,-} n_{\mu}g_{\mu}^{jk}E_k \\ &\quad - \kappa E_j - \sum_{k=+,-} \tilde{\gamma}_{jk}E_k, \end{aligned} \quad (53)$$

$$\begin{aligned} \frac{d}{dt}n_{\mu} &= -\gamma_{\parallel}(n_{\mu} - n_{0\mu}) - \gamma_J(n_{\mu} - n_{\mu'}) \\ &\quad - \tilde{\mathcal{G}}\tilde{\Gamma} \sum_{k=+,-} \sum_{l=+,-} \text{Re}\{g_{\mu}^{kl}E_k^*E_l\}n_{\mu}, \end{aligned} \quad (54)$$

where the notation $\tilde{\gamma}_{jk} = \mathcal{I}^{-1}\gamma_{jk}$ and $\tilde{\Gamma} = \mathcal{I}^{-1}\mathcal{W}$ is introduced.

B. Spin-flip model with linear gain anisotropy

The important consequence of Eqs. (53) and (54) is the possibility to derive the extension of the well-known SFM to some more-general situations. (i) We extend the SFM to include gain anisotropy different from circular gain dichroism (due to spin-carrier imbalance), such as the linear gain dichroism due to strain inside a QW. (ii) The second extension originates from the fact that the cavity-related quantities, such as anisotropy rates, can be calculated self-consistently. This provides a clear rigorous background to the SFM. (iii) Moreover, the extended SFM can be straightforwardly generalized to respect the shape of the optical mode within the cavity, especially in the active region.

To derive the extended SFM, the field and population variables must be rescaled in an appropriate way. To do so, we introduce the populations N and m and mode amplitudes A_{\pm} , in a similar manner as San Miguel *et al.* [30], defined as

$$\begin{aligned} n_{\uparrow,\downarrow} &= \frac{\kappa}{\mathcal{G}\Gamma}(N \pm m), \\ E_{\pm} &= \sqrt{\frac{2\gamma_{\parallel}}{\tilde{\mathcal{G}}\tilde{\Gamma}}}A_{\pm}\exp(-i\alpha\kappa t). \end{aligned} \quad (55)$$

We get rid of fundamental constants and coupling coefficients, keeping just the main structure of the rate equations necessary for a description of important laser features.

Before we find the rate equations for A_{\pm} , N , and m , it is useful to study the polarization-dependent coefficients g_{μ}^{jk} . Because of the specific basis we have chosen, and the relatively small values of the gain-anisotropy parameter \mathcal{D} (up to $\mathcal{D} = 0.1$), we can ignore two of them; namely, g_{\uparrow}^{--} and g_{\downarrow}^{++} . From the definition, it can be shown that they are equal to each other: $\mathbf{e}_{-}^{\dagger}\hat{\mathcal{T}}_{\uparrow}\mathbf{e}_{-} = \mathbf{e}_{+}^{\dagger}\hat{\mathcal{T}}_{\downarrow}\mathbf{e}_{+} = \mathcal{D}^2/(1 + \mathcal{D}^2)$.

The remaining coefficients g_{μ}^{jk} take only two different values, and according to calculations, we define $g = 1/(1 + \mathcal{D}^2)$ and $\tilde{g} = 2\mathcal{D}/(1 + \mathcal{D}^2)$.

Thus, the relations from Eq. (55) are applied to Eqs. (53) and (54), from which one obtains, after performing simple algebraic operations, the so-called extended spin-flip model:

$$\begin{aligned} \dot{A}_{+} &= \kappa(1 - i\alpha) \{[g(N + m) - 1]A_{+} + \tilde{g}NA_{+}\} \\ &\quad - \tilde{\gamma}_{++}A_{+} - \tilde{\gamma}_{+-}A_{-}, \end{aligned} \quad (56)$$

$$\begin{aligned} \dot{A}_{-} &= \kappa(1 - i\alpha) \{[g(N - m) - 1]A_{-} + \tilde{g}NA_{+}\} \\ &\quad - \tilde{\gamma}_{--}A_{-} - \tilde{\gamma}_{-+}A_{+}, \end{aligned} \quad (57)$$

$$\begin{aligned} \dot{N} &= \gamma_{\parallel}(N_0 - N) - \gamma_{\parallel} \{[g(I_{+} + I_{-}) + \tilde{g}I_{\pm}]N \\ &\quad + g(I_{+} - I_{-})m\}, \end{aligned} \quad (58)$$

$$\begin{aligned} \dot{m} &= \gamma_{\parallel}\mathcal{P}_JN_0 - (\gamma_{\parallel} + 2\gamma_J)m - \gamma_{\parallel} \{[g(I_{+} + I_{-}) + \tilde{g}I_{\pm}]m \\ &\quad + g(I_{+} - I_{-})N\}, \end{aligned} \quad (59)$$

where the optical intensities $I_{+} = |A_{+}|^2$, $I_{-} = |A_{-}|^2$, and $I_{\pm} = 2\text{Re}\{A_{\pm}^*A_{\mp}\}$ are defined. The overall pumping rate is described by the unsaturated carrier concentration N_0 . The fact that the linewidth enhancement factor α may be polarization dependent is ignored here.

In the absence of any linear gain anisotropy ($\mathcal{D} = 0$), the coefficients g and \tilde{g} reduce to $g = 1$ and $\tilde{g} = 0$, which gives the conventional SFM with generalized anisotropy rates $\tilde{\gamma}_{ij}$, which consist of the birefringence rate γ_p and the dichroism rate γ_a as a special case, as shown later.

One of the predictions of the extended SFM is an additional contribution to the total frequency splitting between linear lasing modes. It is due to phase-amplitude coupling in the presence of the linear gain anisotropy \mathcal{D} . A standard derivation leads to the approximate expression

$$\delta\omega \approx 2\alpha\kappa\mathcal{D}, \quad (60)$$

which is valid for small values of \mathcal{D} , which is formally equivalent to a general expression given in the literature for such a kind of anisotropy [59].

One can expect effects arising due to $\mathcal{D} \neq 0$. Detailed qualitative analysis of the extended SFM, such as bifurcation analysis or calculation of the modulation response, is beyond the scope of the present paper. Nevertheless, gain anisotropy should strongly influence the beating frequency between circular modes.

It is important to note that if we use a different basis to derive the extended SFM, we will obtain a different set of differential equations. However, the physics that is modeled would be the same as long as we ignore terms in the second order of gain anisotropy \mathcal{D} .

C. Linear birefringence and dichroism rates

The mathematical framework developed in this paper allows one to calculate realistic values of anisotropy rates such as the birefringence rate γ_p and the dichroism rate γ_a . They can be calculated not only using the rigorous matrix formalism [19], which is reformulated in this paper, but more importantly in a self-consistent way within the framework of the time-dependent coupled-mode theory. This subsection is based on the computational rules, introduced in Sec. IV C. We derive approximate analytic expressions for γ_p and γ_a , which may provide useful physical insights.

To derive and validate this approach, we consider a single-QW structure, as depicted in Fig. 5. For simplification, this structure contains only a single anisotropic layer (apart from the possible anisotropies in the active layer), which is placed in two different locations within the optical cavity. This is emphasized by respective red and blue layers with reduced coordinates $\zeta = 0.1$ and $\zeta = 0.15$ in the local reference frame, as shown in the inset. We write down the permittivity tensor of such a layer without z components, since the off-axis wave propagation along z is ignored here. The permittivity tensor is expressed in the $\{[110], [1\bar{1}0]\}$ basis according to

$$\hat{\varepsilon}_A = \begin{bmatrix} \varepsilon_{A,xx} & 0 \\ 0 & \varepsilon_{A,yy} \end{bmatrix}. \quad (61)$$

Next we consider a particular linear birefringence and linear dichroism inside a given layer. Material birefringence and dichroism are quantified using parameters $\delta\varepsilon_r$ and $\delta\varepsilon_i$, respectively: $\delta\varepsilon_r = \text{Re}\{\varepsilon_{A,xx} - \varepsilon_{A,yy}\}$ and $\delta\varepsilon_i = \text{Im}\{\varepsilon_{A,xx} - \varepsilon_{A,yy}\}$. Both parameters are positive real numbers by convention. We calculate the off-diagonal normalized matrix

element $\tilde{\gamma}_{+-}$ of the anisotropy operator $\hat{\gamma}$. Using Eq. (49), we obtain

$$\tilde{\gamma}_{+-} = -i\frac{\omega}{2}\Gamma_A \left[\mathbf{e}_+^\dagger (\hat{\varepsilon}_A^{-1}) \mathbf{e}_- \right] \varepsilon_A, \quad (62)$$

where Γ_A stands for the optical confinement factor of the anisotropic layer and ε_A is the absolute value of the isotropic part of the permittivity tensor. Straightforward calculation, in which the convention $\mathbf{e}_\pm = [1, \mp i]^T / \sqrt{2}$ is used, leads to

$$\tilde{\gamma}_{+-} = \Gamma_A \frac{\omega}{2} \left(\frac{\delta\varepsilon_i + i\delta\varepsilon_r}{2\varepsilon_{A,xx}\varepsilon_{A,yy}} \right) \varepsilon_A. \quad (63)$$

To simplify this expression for $\tilde{\gamma}_{+-}$, we use the approximation $\varepsilon_{A,xx}\varepsilon_{A,yy} \approx \varepsilon_A^2$, which is valid in the case of $\delta\varepsilon_{r,i} \ll \varepsilon_A$. In this approximation, one can see that the expression we derive consists of real and imaginary parts. We show numerically, that this can be interpreted in the following way: $\text{Re}\{\tilde{\gamma}_{+-}\} = \gamma_a$ and $\text{Im}\{\tilde{\gamma}_{+-}\} = \gamma_p$. Namely, the real and imaginary parts of $\tilde{\gamma}_{+-}$ are equal to the dichroism rate γ_a and the birefringence rate γ_p , respectively. They are given approximately by the simple relations

$$\begin{aligned} \gamma_a &\approx \Gamma_A \left(\frac{\omega}{2} \right) \frac{\delta\varepsilon_i}{2\varepsilon_A}, \\ \gamma_p &\approx \Gamma_A \left(\frac{\omega}{2} \right) \frac{\delta\varepsilon_r}{2\varepsilon_A}. \end{aligned} \quad (64)$$

Such formulas are rather intuitive concerning polarization anisotropies in VCSELs, but also agree qualitatively with alternative, but incomplete, expressions derived in the past to some extent [25,38].

D. Numerical validation

In this section, we compare the predictions of analytic expressions directly with the rigorous matrix formalism (see Sec. III), showing the robustness of our coupled-mode theory implemented here. We focus now on the numerical predictions of experimentally related quantities such as the frequency splitting between orthogonal linear modes in the absence of any spin injection. Another quantity of interest is the splitting of threshold pump rates, or threshold carrier concentrations of such modes. Finally, the polarization state of emitted modes is studied.

The formalism is demonstrated on a single-QW spin-VCSEL structure, as depicted in Fig. 5. It consists of a single active layer with thickness $d_{\text{QW}} = 10$ nm, which models the QW. The short cavity is placed between two Bragg mirrors, composed of 15 units of GaAs/AlAs and 25 units of AlAs/GaAs, respectively, and designed for a wavelength λ of around $1.005 \mu\text{m}$. Apart from the active layer, the cavity contains an anisotropic layer of thickness $d_A = 25$ nm, with linear birefringence and linear dichroism

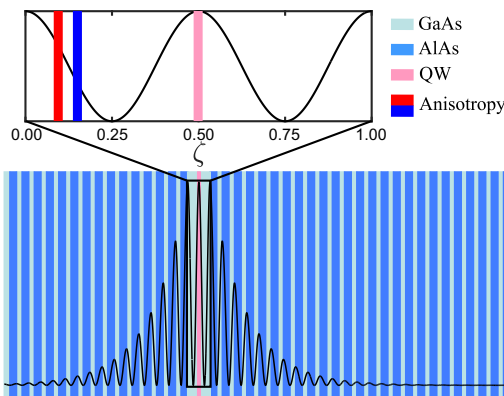


FIG. 5. A simple single-QW structure used for numerical validation, with the electric field distribution calculated using the modified matrix formalism. The inset shows the position of the active layer and two possible positions [red ($\zeta = 0.1$), blue ($\zeta = 0.15$)] of the anisotropic passive layer within the λ -cavity field. The local reference frame is described by ζ .

described by nonzero $\delta\varepsilon_r$ and $\delta\varepsilon_i$. The optical constants are $\varepsilon_{\text{GaAs}} = 12.25$, $\varepsilon_{\text{AlAs}} = 8.68$, $\varepsilon_{\text{QW}} = 12.96$, and $\varepsilon_A = \varepsilon_{\text{GaAs}}$ [60]. We show how some of main consequences of even the smallest change in the geometry of the device can be predicted with sufficiently high precision. It is shown in Sec. VI how exactly the anisotropic elements inside the laser cavity can be technologically important.

1. Frequency splitting

We now consider the given single-QW structure free of any anisotropies beside linear birefringence. It can be derived using Eq. (64) that the frequency splitting is given by $\delta\nu/\nu \approx (\Gamma_A/2) \delta\varepsilon_r/\varepsilon_A$. Direct numerical comparison with calculation based on our matrix formalism is shown in Fig. 6(a). Particular colors of the lines refer to the position

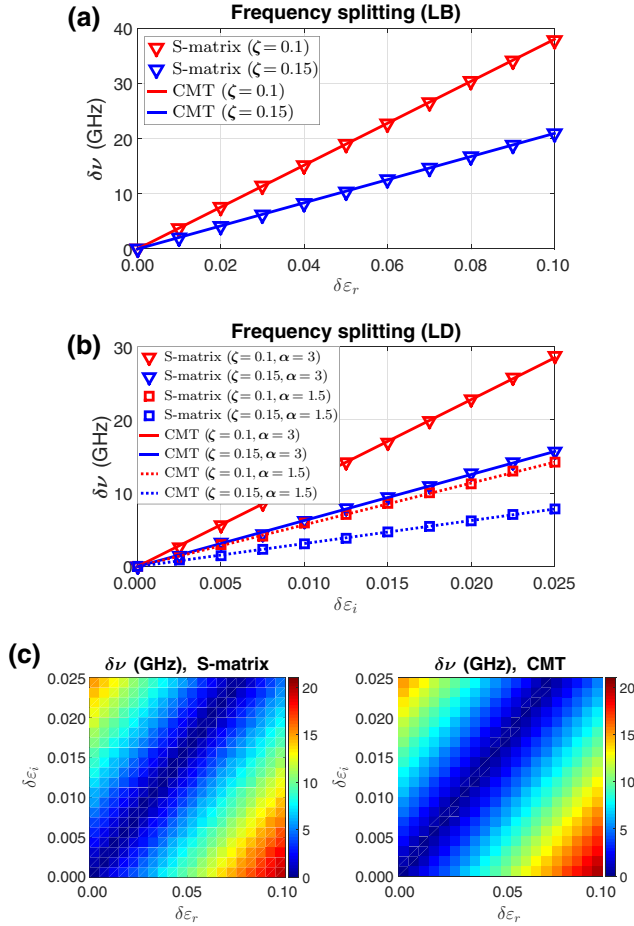


FIG. 6. Frequency splitting calculated as a function of the linear birefringence (LB) parameter $\delta\varepsilon_r$ (a), of the linear dichroism (LD) parameter $\delta\varepsilon_i$, due to a nonzero Henry factor α (b), and of both anisotropy parameters (c). The results obtained with our scattering matrix (*S*-matrix) formalism are used as a reference to evaluate the precision of the method, based on coupled-mode theory (CMT).

of the anisotropic layer within the optical field according to Fig. 5. The values of the confinement factor of the anisotropic layer are $\Gamma_{\text{red}} = 0.0312$ and $\Gamma_{\text{blue}} = 0.0172$. We find perfect agreement between the two methods.

Another contribution to the frequency splitting originates from the phase-amplitude coupling. In this case, the extended SFM predicts the value $\delta\nu/\nu \approx \alpha (\Gamma_A/2) \delta\varepsilon_i/\varepsilon_A$. Note that the birefringence in the layer is switched off: $\delta\varepsilon_r = 0$. The results, together with the comparison with the rigorous matrix method, are depicted in Fig. 6(b). Two different realistic values of the Henry factor α are used, so the magnitude of phase-amplitude coupling can be controlled. Quantitatively, the results are in perfect agreement.

Finally, the combined contribution of both local anisotropy parameters $\delta\varepsilon_r$ and $\delta\varepsilon_i$ is studied. The absolute value of the frequency difference is $\delta\nu/\nu \approx (\Gamma_A/2) |\delta\varepsilon_r - \alpha \delta\varepsilon_i|/\varepsilon_A$. Very good agreement between both methods is obtained, as shown in Fig. 6(c). The results are calculated for $\zeta = 0.15$.

Calculations using the linear basis functions are performed as well. We decide to use the option of two orthogonal linearly polarized basis functions with degenerate frequencies. In this case, the coupled-mode theory gives results almost identical to those obtained with a circular basis.

2. Threshold splitting

The calculation concerning the effects of anisotropies on lasing threshold is not as straightforward as in the case of frequency splitting. The validity of coupled-mode theory may be determined by calculating the ratio $N_{[110]}/N_{[1\bar{1}0]}$, where $N_{[110]}$ and $N_{[1\bar{1}0]}$ are the threshold carrier concentrations for linear laser modes oscillating along the $[110]$ and $[1\bar{1}0]$ crystallographic axes, respectively. The prediction of the spin-flip model is $N_{[110]}/N_{[1\bar{1}0]} = (\kappa - \gamma_a)/(\kappa + \gamma_a)$. In the case of the matrix formalism, one has to calculate the ratio $\bar{\chi}_{[110]}/\bar{\chi}_{[1\bar{1}0]}$ since $\bar{\chi} \propto N_\uparrow + N_\downarrow$ or equivalently $N_{0\uparrow} + N_{0\downarrow}$, because we consider a laser at or near threshold. The results, depicted in Fig. 7(a), show excellent agreement for $\delta\varepsilon_i < 0.015$.

Next we consider the optical anisotropies located solely inside the active layers: circular gain dichroism, induced by electron spin imbalance, and linear gain dichroism. We ignore any additional passive anisotropies now. One should expect significant differences in the pumping rates at the respective thresholds (or threshold carrier concentrations) of particular modes in the presence of gain anisotropies.

Figure 7(b) displays the calculation of $N_{[110]}/N_{[1\bar{1}0]}$, where $N_{[110]} = 1/(g + \tilde{g})$ and $N_{[1\bar{1}0]} = 1/(g - \tilde{g})$ according to the extended spin-flip model. \mathcal{D} is an adjustable parameter. In the language of permittivities, one derives $\delta\varepsilon_{a,i} = 2 \bar{\chi} \mathcal{D}$, where $\delta\varepsilon_{a,i}$ is the difference of imaginary parts of permittivities along anisotropy principal axes (see

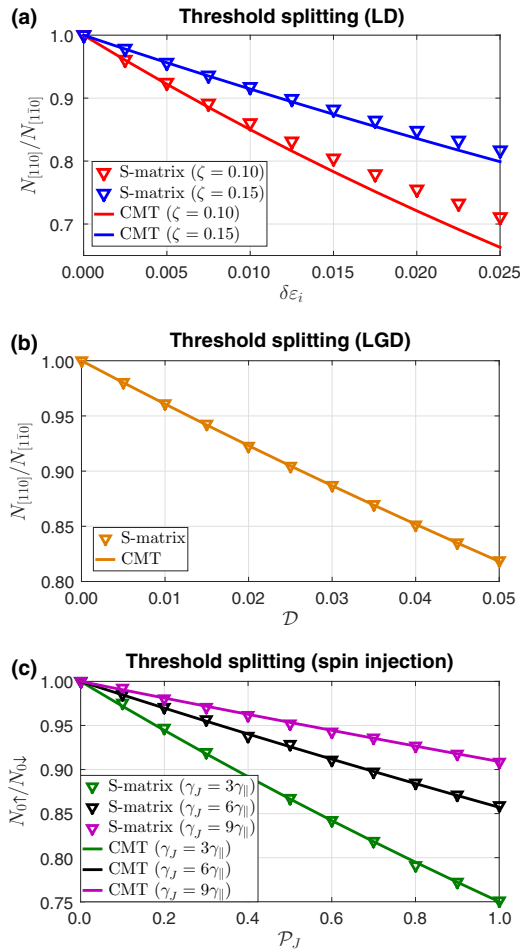


FIG. 7. (a) Calculated $N_{[110]}/N_{[1\bar{1}0]}$ ratio as a function of the linear dichroism (LD) parameter $\delta\epsilon_i$. (b) The calculated $N_{[110]}/N_{[1\bar{1}0]}$ ratio as a function of the linear gain dichroism (LGD) $D = \delta\epsilon_{a,i}/(2\bar{\chi})$. (c) The ratio of threshold pumping rates $N_{0\uparrow}/N_{0\downarrow}$ in the structure with circular gain dichroism, due to electron spin imbalance, but without additional linear anisotropies. S-matrix stands for scattering matrix and CMT for coupled-mode theory.

Sec. III). Numerical values obtained with our extended SFM are in excellent agreement with those extracted with the matrix formalism. A similar calculation is performed for circular modes under spin-polarized pumping (P_J) for several values of the spin-mixing rate γ_J .

3. Polarization eigenmodes at the threshold

Next we show that our extended SFM gives good results even concerning the polarization state of possible threshold modes, which may be the most general in this case. We consider the linear birefringence and linear dichroism in the passive layer, linear gain anisotropy in the active layer, and additionally spin-polarized electron injection. A very similar calculation was presented in our previous contribution [61], in which we used the scattering-matrix

formalism to extract dynamics-related quantities for the conventional SFM. However, in this case, our extended SFM based on coupled-mode theory is computationally self-consistent. Thus, the results of the robust matrix formalism are not required to obtain comparable results.

We transform equations for field amplitudes from the extended SFM to the $\{\mathbf{x}, \mathbf{y}\}$ basis, in which the field-amplitude components are $\mathbf{A} = [A_x, A_y]^T$. The resulting rate equations can be expressed compactly as $\partial_t \mathbf{A} = \hat{\Omega} \mathbf{A}$, where $\hat{\Omega}$ is a certain time-evolution operator. It can be shown that the polarization eigenmodes we are looking for are the eigenvectors of the operator $\hat{\Omega}$.

Analytically extracted eigenvectors are used to calculate components of the Stokes vector \mathcal{S} as functions of the spin-injection polarization degree P_J and birefringence parameter $\delta\epsilon_r$ (and the small dichroism $\delta\epsilon_i = \delta\epsilon_r/10$) with fixed $D = 0.025$, $\gamma_{\parallel} = 1$ GHz, and $\gamma_J = 3\gamma_{\parallel}$, which belongs to the range of values observed experimentally at lower temperatures [62]. Otherwise, at room temperatures, the values of γ_J are usually larger, ranging from several gigahertz to hundreds of gigahertz, which is beneficial for

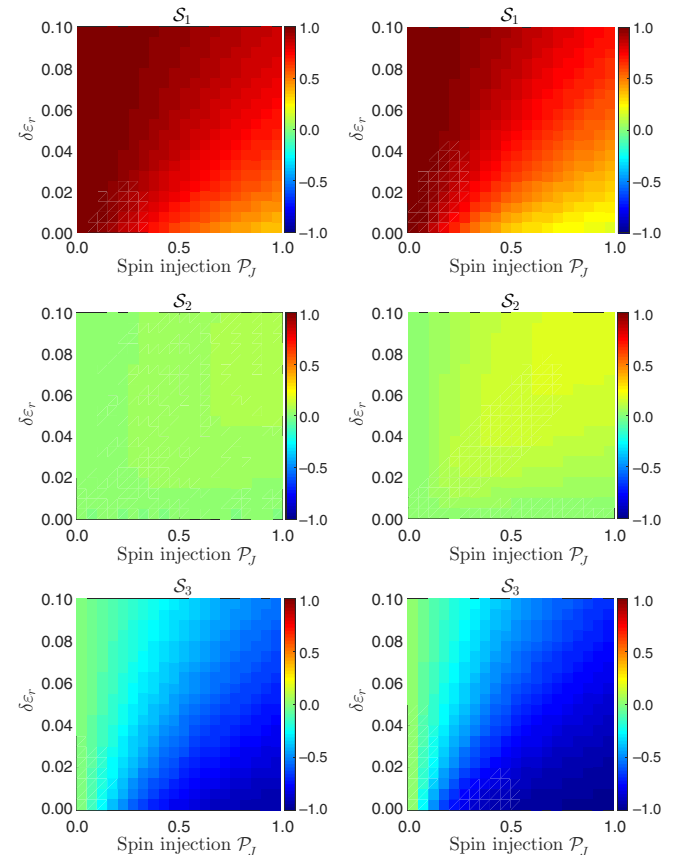


FIG. 8. Components of the reduced Stokes vector $\mathcal{S} = [S_1, S_2, S_3]^T$ of a single laser eigenmode calculated with the rigorous matrix formalism (left) and with the extended spin-flip model based on the coupled-mode theory (right).

the field of ultrafast spin lasers [30,63,64]. The results are shown in Fig. 8, together with refined calculations based on the scattering-matrix formalism. We use the approximation $N \approx 1$. Compared with the results from Ref. [61], in which we compared the matrix approach with the conventional spin-flip model, one can see that separation of amplitude anisotropy into passive (linear dichroism) and active (linear gain anisotropy) contributions increases the precision.

VI. APPLICATION: SPIN-VCSELS FOR TERAHERTZ SOURCES AND ULTRAFAST DATA TRANSMISSION

In this section, we apply the theoretical tools developed to design and optimize conceptual spin-VCSEL structures with a one-dimensional grating, which locally induces extremely large linear birefringence and thus large frequency splitting between coexisting electric field components. It is an alternative option to recently demonstrated methods based on heating or bending the structures, where a frequency splitting $\delta\nu$ of 214 GHz was achieved [13,65]. More recently, by implementation of a surface grating, $\delta\nu \approx 100$ GHz was obtained [66,67]. Even higher $\delta\nu$ can be obtained using one-dimensional grating-based reflectors, but for the price of very large losses of the weaker mode. This can be solved with use of a properly designed two-dimensional grating.

Considering spin-VCSELS, the combination of very high anisotropies in the cavity, resulting in a large frequency splitting, and extremely large spin-mixing rate, as observed at room temperatures, offers an unique advantage in the dynamic performance over conventional devices. This applies to potential and very promising applications, such as ultrafast data transmission and generation of terahertz radiation.

A. Spin lasers with subwavelength gratings

To achieve frequency splitting in the terahertz range, we use the numerical recipe introduced in Sec. III to design the conceptual spin-VCSEL structures with highly anisotropic subwavelength gratings. In the following, we demonstrate the potential of spin lasers for terahertz generation by two approaches: (i) a structure with an intracavity grating and (ii) a structure with a surface grating. The ultrafast polarization modulation is then discussed for the intracavity design with the possibility of good integration in compact devices.

1. Structure with an intracavity grating

We propose a structure with a high-contrast intracavity grating, as shown in Fig. 9(a). It is based on a resonant 2λ cavity made of GaAs, with four (In,Ga)As QWs and an (Al,Ga)As/air grating. The Bragg mirrors are made of 15

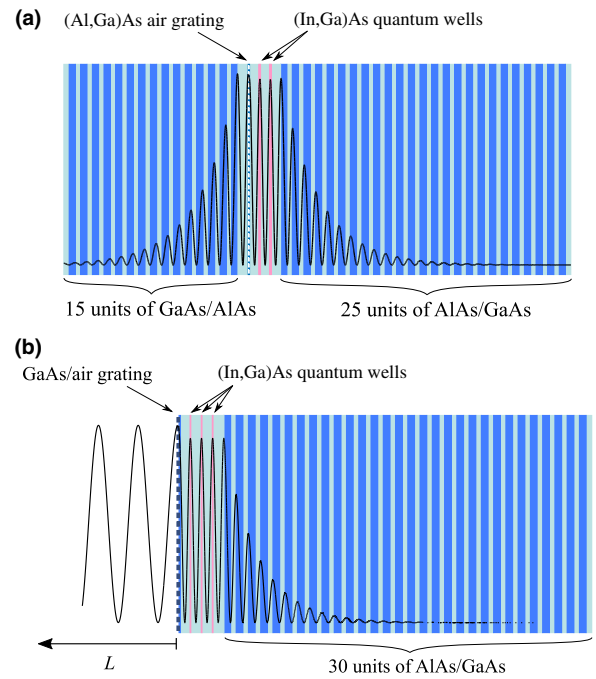


FIG. 9. (a) A $\lambda = 1300$ nm VCSEL with four (In,Ga)As QWs and an intracavity (Al,Ga)As/air grating and (b) a $\lambda = 940$ nm half-VCSEL with three (In,Ga)As QWs, a GaAs/air surface grating, and a microcavity of length L .

units of GaAs/AlAs and 25 units of AlAs/GaAs, respectively. The structure is optimized to emit light at wavelength $\lambda \approx 1300$ nm. The optical constants used in the design are $\varepsilon_{\text{GaAs}} = 11.56$, $\varepsilon_{\text{AlAs}} = 8.41$, $\varepsilon_{(\text{In,Ga})\text{As}} = 12.32$, and $\varepsilon_{(\text{Al,Ga})\text{As}} = 10.69$ [60].

Structures of this type are usually fabricated in three steps: (i) initial epitaxial growth of a substrate Bragg mirror and a multiple-QW active region, (ii) fabrication of the grating by, for example, electron-beam lithography, and (iii) epitaxial regrowth of the rest of the structure [68,69]. Wafer bonding is an alternative method of preparation [70].

2. Microcavity structure with a surface grating

The second structure designed for $\lambda \approx 940$ nm, depicted in Fig. 9(b), consists of three (In,Ga)As QWs and a GaAs/air grating at the surface of a half-VCSEL inside the microcavity similar to those of MEMS VCSELS. The Bragg mirror is made of 30 units of AlAs/GaAs. The optical constants corresponding to the emission wavelength are $\varepsilon_{\text{GaAs}} = 12.6$, $\varepsilon_{\text{AlAs}} = 8.76$, and $\varepsilon_{(\text{In,Ga})\text{As}} = 13.18$ [60].

B. Terahertz-radiation generation

Existing terahertz sources are too large, or they can operate only at cryogenic temperatures. Alternatively, they require the use of more than one external laser. Such disadvantages could be eventually solved using highly

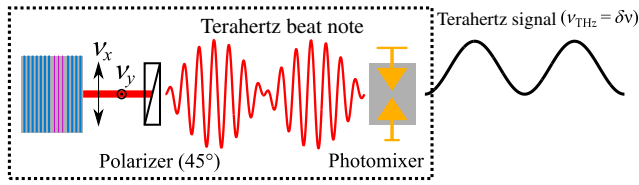


FIG. 10. Compact source of monochromatic terahertz radiation based on a highly anisotropic spin laser.

anisotropic spin lasers, in which the beat-node signal in the terahertz range coming from interference of orthogonally polarized modes could be used to generate terahertz radiation by means of photomixing [14]. The proposed source of terahertz radiation is schematically shown in Fig. 10. The role of spin injection here is to allow the simultaneous oscillation of both polarization components and potentially to slightly tune the frequency splitting and consequently the frequency of the terahertz wave ($\nu_{\text{THz}} = \delta\nu$).

We use the effective-medium approximation, which is valid for long wavelengths [71], to describe the effective anisotropy of grating. For simplicity, we consider the grating to be the only source of anisotropy. In the case of a lamellar grating, the ordinary and extraordinary permittivities ϵ_o and ϵ_e are given by $\epsilon_o = f \epsilon_a + (1 - f) \epsilon_b$ and $\epsilon_e^{-1} = f \epsilon_a^{-1} + (1 - f) \epsilon_b^{-1}$, where f is the fill factor and ϵ_a and ϵ_b are bulk permittivities of the two materials composing the grating [72].

The frequency splitting induced by the grating, calculated by our using proposed matrix formalism, is shown in Fig. 11(a) for variable grating thickness and fill factor. We show that with an intracavity grating [see Fig. 9(a)] it is possible to achieve frequency splitting $\delta\nu > 1$ THz if one correctly chooses the grating geometry and material. We achieved frequency splitting of orthogonal linear modes close to 1.4 THz for grating fill factor $f = 0.75$ and a thickness of 25 nm.

For the case of a microcavity spin-injected vertical-external-cavity surface-emitting laser with a surface grating [see Fig. 9(b)], we show the results in Fig. 11(b). We keep the fill factor $f = 0.5$. The calculation shows the effects of variable grating thickness and microcavity length L . The values of $\delta\nu$ obtained surpass the results obtained for a monolithic spin-VCSEL for two reasons. First, most of the cavity consists of air, and second, the permittivity of the GaAs grating is larger than that of (Al,Ga)As at the given wavelengths.

C. Polarization modulation for ultrafast communication

The utilization of the polarization degree of freedom opens horizons to surpass conventional current-driven intensity-modulated VCSELs, in which the modulation

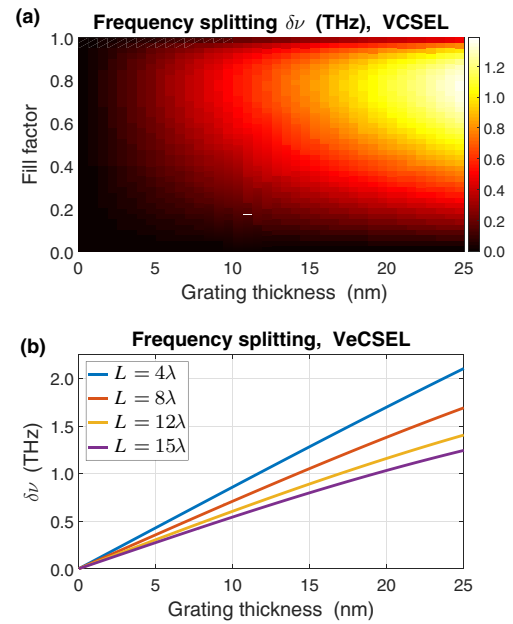


FIG. 11. (a) Frequency splitting between orthogonally polarized laser modes as a function of intracavity (Al,Ga)As grating thickness and fill factor. (b) Frequency splitting of modes in a vertical-external-cavity surface-emitting laser (VeCSEL) with a GaAs surface grating and a microcavity as a function of grating thickness and microcavity length L .

performance depends, for example, on the cavity decay rate κ and the pump current, limiting room-temperature-modulation bandwidths to approximately 35 GHz [73]. Similarly, in the case of polarization dynamics, the crucial quantity here is the phase anisotropy rate γ_p . The larger γ_p is, the faster temporal switching between circular polarization modes occurs.

Naturally, the possibility of encoding the information into the polarization state of light arises. While in the case of intensity-modulated conventional VCSELs, bits “0” and “1” are reached by the laser being below and above threshold, respectively, in the case of polarization-modulated spin-VCSELs, bits are encoded as an opposite injected spin and thus emitted orthogonal circular polarizations. Such modulation, which is needed for high-speed information transfer, could be performed by means of time-varying injection of spin current either optically or electrically. Recently, fast pulsed optical spin injection has been demonstrated in an array of VCSELs with large birefringence induced by bending [13]. From the spintronic point of view, the challenge is to develop an integrated method for fast modulation (in the range from hundreds of gigahertz up to terahertz) of electrically injected spin current [74].

Figure 12 shows the simulated polarization modulation described by the degree of circular polarization

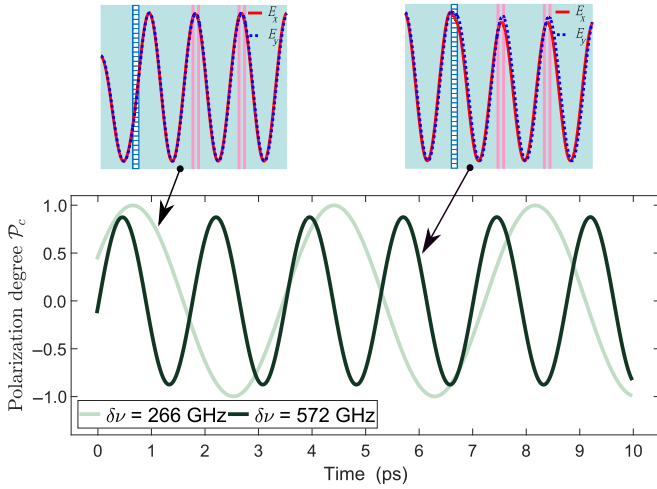


FIG. 12. Simulated polarization modulation of a spin-VCSEL with a grating for two different positions of the grating within the cavity.

$\mathcal{P}_c(t) = [I_+(t) - I_-(t)]/[I_+(t) + I_-(t)]$. We study two different positions of the grating within the cavity. The parameters used in simulations are $N_0 = 5$, $\alpha = 3$, $\gamma_{\parallel} = 1$ GHz, $\kappa = 133$ GHz, $g = 1$, $\tilde{g} = 0$ ($\mathcal{D} = 0$), and fill factor $f = 0.25$ in both cases. The birefringence rate is extracted from the value of the frequency splitting as $\gamma_p = \pi \delta\nu$. The spin modulation is introduced as $\mathcal{P}_J(t) = \mathcal{A}_J \cos(2\pi f_m t)$, with amplitude $\mathcal{A}_J = 0.5$ and frequency f_m matching the frequency splitting due to birefringence. The harmonic signal can, in principle, be replaced by the string of bits. The speed of polarization modulation is limited by the spin-mixing rate γ_J , which is chosen to be $500\gamma_{\parallel}$ here. Nowadays, there is a significant experimental effort to make the spin-mixing rate as large as possible, in contrast to conventional spintronics. The field of ultrafast spin lasers can thus benefit from the fact that the spin-mixing rate increases with temperature [64].

Figure 12 also demonstrates strong sensitivity of the resulting polarization-modulation speed to the location of the grating layer in the multilayer structure. One can see that even a very small shift in the position of the grating leads to a very large change of polarization-degree oscillations. Soon, our theoretical framework will be extended to structures with lateral periodicity by incorporation of rigorous coupled-wave analysis, for which our approach is well suited [75].

VII. CONCLUSION AND PERSPECTIVES

We formulate the semiclassical model of a spin laser with particular focus on local optical anisotropies and highly birefringent structures. It is used to develop the steady-state robust matrix description of spin-VCSELs. This can be further generalized to describe the steady-state operation of spin-VCSELs pumped above threshold,

including saturation effects. It will be important to use a more-realistic description of QW gain and include lateral effects in electromagnetic wave propagation. This will allow the study of mode competition in a rigorous way. For terahertz applications, it is suitable for direct implementation of periodic structures such as birefringent gratings by means of rigorous coupled-wave analysis. The semiclassical model is also used to develop coupled-mode theory, which allows one to treat spin-VCSEL structures layer-by-layer. It is sensitive to any small changes in optical and geometric properties of the laser cavity and gain media. We use the vectorial eigenmodes of active structures, extracted using the matrix formalism, in contrast to previous approaches. The only input parameters are the optical and geometric properties of particular layers. Our model leads to the extended spin-flip model with polarization-dependent gain. In the future, it will be worth performing detailed analysis of the effects arising from additional terms due to linear gain anisotropy.

In this paper, we proposed and design conceptual spin-VCSEL structures with birefringent gratings. For simplicity, we use the one-dimensional approximation, ignoring any effects of lateral confinement, which is beyond the scope of the present paper. However, it is important to note that the scattering-matrix formalism, in the frame of aperiodic rigorous coupled-wave analysis or the method of lines, as well as the coupled-mode theory can be formulated in higher dimensions, which will be the objective of our future work. Such structures have potential to be of significant importance for terahertz photonics: (i) as compact tunable sources of terahertz radiation and (ii) as ultrafast polarization modulators for data transfer. The robust matrix formalism together with coupled-mode theory is proven to be a precise tool for the design and optimization of future spin-VCSEL structures.

ACKNOWLEDGMENTS

We thank Fabien Bretenaker for fruitful discussions. Support from the projects IT4 Innovations National Supercomputing Center Path to Exascale Project No. CZ.02.1.01/0.0/0.0/16 013/0001791 and Student Project No. SP2020/150 and the Czech Science Foundation Grant No. 18-22102S is acknowledged.

APPENDIX A: TRANSFER-MATRIX AND SCATTERING-MATRIX FORMALISM

Steady-state electromagnetic field propagation inside multilayer structures such as spin-VCSELs can be efficiently described using Yeh's matrix approach. The basic idea is that one solves the wave equation for each layer separately and these solutions are connected by applying relevant boundary conditions. The frequency-domain wave equation for the electric field amplitude $\mathbf{E}_0^{(n)}$ inside

any general anisotropic medium is

$$\mathbf{W}^{(n)} \mathbf{E}_0^{(n)} = 0, \quad (\text{A1})$$

where $\mathbf{W}^{(n)} = (\omega/c)^2 \hat{\epsilon}^{(n)} - [\mathbf{q}^{(n)}]^2 + \mathbf{q}^{(n)} \otimes [\mathbf{q}^{(n)}]^T$ is the wave-equation operator with the permittivity tensor $\hat{\epsilon}^{(n)}$ and wave vector $\mathbf{q}^{(n)}$ specific for each layer. The z components of $\mathbf{q}^{(n)}$ are extracted from the condition for the nontrivial solution:

$$\det[\mathbf{W}^{(n)}] = 0. \quad (\text{A2})$$

Because of the symmetry of the class of media considered, one obtains four propagation constants $\mathbf{q}_{zj}^{(n)}$, where $j = 1, 3$ refer to forward-propagating modes and $j = 2, 4$ refer to backward-propagating modes. Solving Eq. (A1) gives particular amplitudes $\mathbf{E}_{0j}^{(n)} = A_j^{(n)} \mathbf{e}_j^{(n)}$, where $\mathbf{e}_j^{(n)}$ is the eigenpolarization vector.

Boundary conditions at the interface between the $(n-1)$ th and (n) th layers can be expressed using matrices as

$$\mathbf{D}^{(n-1)} \mathbf{A}^{(n-1)} = \mathbf{D}^{(n)} \mathbf{P}^{(n)} \mathbf{A}^{(n)}, \quad (\text{A3})$$

where $\mathbf{A}^{(n)}$ is the vector of amplitudes, and $\mathbf{D}^{(n)}$ and $\mathbf{P}^{(n)}$ are the dynamic and propagation matrix, respectively. They are given by

$$\mathbf{D}^{(n)} = \begin{bmatrix} \mathbf{e}_{x1}^{(n)} & \mathbf{e}_{x2}^{(n)} & \mathbf{e}_{x3}^{(n)} & \mathbf{e}_{x4}^{(n)} \\ \mathbf{h}_{y1}^{(n)} & \mathbf{h}_{y2}^{(n)} & \mathbf{h}_{y3}^{(n)} & \mathbf{h}_{y4}^{(n)} \\ \mathbf{e}_{y1}^{(n)} & \mathbf{e}_{y2}^{(n)} & \mathbf{e}_{y3}^{(n)} & \mathbf{e}_{y4}^{(n)} \\ \mathbf{h}_{x1}^{(n)} & \mathbf{h}_{x2}^{(n)} & \mathbf{h}_{x3}^{(n)} & \mathbf{h}_{x4}^{(n)} \end{bmatrix}, \quad (\text{A4})$$

$$\mathbf{P}^{(n)} = \begin{bmatrix} e^{i\mathbf{q}_{z1}^{(n)} d^{(n)}} & 0 & 0 & 0 \\ 0 & e^{i\mathbf{q}_{z2}^{(n)} d^{(n)}} & 0 & 0 \\ 0 & 0 & e^{i\mathbf{q}_{z3}^{(n)} d^{(n)}} & 0 \\ 0 & 0 & 0 & e^{i\mathbf{q}_{z4}^{(n)} d^{(n)}} \end{bmatrix}, \quad (\text{A5})$$

where $\mathbf{h}_j^{(n)}$ are the magnetic field eigenpolarizations and $d^{(n)}$ stands for the thickness of the n th layer. Each layer can be described by its own characteristic matrix $\mathbf{T}^{(n)} = \mathbf{D}^{(n)} \mathbf{P}^{(n)} [\mathbf{D}^{(n)}]^{-1}$. All of the layers contained within the structure can be recursively connected and the amplitudes $\mathbf{A}^{(0)}$ and $\mathbf{A}^{(N+1)}$ are related as $\mathbf{A}^{(0)} = \mathbf{M} \mathbf{A}^{(N+1)}$, where \mathbf{M} is the total matrix:

$$\mathbf{M} = [\mathbf{D}^{(0)}]^{-1} \left\{ \prod_{l=1}^N \mathbf{T}^{(l)} \right\} \mathbf{D}^{(N+1)}. \quad (\text{A6})$$

Alternatively, the scattering matrix \mathbf{S} of the system can be derived in a similar way, relating outgoing and incoming amplitudes: $\mathbf{A}_{\text{out}} = \mathbf{S} \mathbf{A}_{\text{in}}$.

APPENDIX B: CALCULATION OF FIELD DECAY RATE κ

1. Standard method based on complex frequency

The total field decay rate κ can be calculated rigorously within the framework of the transfer-matrix or scattering-matrix formalism. It can be done by using the formalism developed in Sec. III. However, the gain of the active layer must be switched off $\bar{\chi} = 0$ and the complex frequency $\tilde{\omega} = \omega - i\kappa$ must be introduced. In the context of the given formalism it has more a sense of artificial gain according to the sign convention. Similarly, also in this case, one is trying to find the values of ω and κ that satisfy the resonance condition [see Eqs. (25) and (27)]. When κ reaches a value equal to the real cavity decay rate, the energy of the cavity mode considered no longer decays [27,76].

2. Analytic method based on the Poynting theorem

Similarly, as in the case of anisotropy rates derived using coupled-mode theory, it is possible to derive simple analytic expressions also for κ . We combine the basic idea behind coupled-mode theory that one can assume the shape of the laser mode with the law of electromagnetic energy conservation, which is the Poynting theorem [77]:

$$\frac{\partial}{\partial t} \int_C u dV = - \oint_{\partial C} \mathbf{S} d\mathcal{A} - \int_C \mathbf{j} \mathbf{E} dV, \quad (\text{B1})$$

where u is the density of the electromagnetic field, \mathbf{S} is the Poynting vector, and \mathbf{j} stands for the density of electric current. If we consider the passive cavity, then it describes the decay of the field due to transmitted light from the structure and internal absorptions. We consider the cavity mode linearly polarized along x or y , described by $\mathbf{E}(z, t) = E(t) \boldsymbol{\varphi}(z)$. Thus, any lateral effects are ignored now. Using the known shape of the cavity mode inside the device, we can derive the following relations. The density of the electromagnetic field inside the cavity with no magnetically active media is $u = \mathbf{E} \mathbf{D} = \varepsilon_0 \varepsilon_m |\boldsymbol{\varphi}|^2 E^2$, where ε_m is the real part of the spatially varying permittivity. The Stokes vector is then $\mathbf{S} = \mathbf{E} \times \mathbf{h} = (\varepsilon_0 c^2 / \omega) |\boldsymbol{\varphi}|^2 E^2 \mathbf{q}$. The absorbing term under the integral is $\mathbf{j} \mathbf{E} = \varepsilon_0 \varepsilon_{m,i} \omega |\boldsymbol{\varphi}|^2 E^2$, where $\varepsilon_{m,i}$ is the imaginary part of the permittivity ($\varepsilon_{m,i} \ll \varepsilon_m$).

Assuming that the entire multilayer structure has length L , one obtains

$$\begin{aligned} & \int_0^{\mathcal{A}_0} \int_0^L \varepsilon_m |\boldsymbol{\varphi}|^2 dz d\mathcal{A} \times \frac{\partial E}{\partial t} \\ &= - \oint_{\partial C} \frac{c^2}{\omega} |\boldsymbol{\varphi}|^2 (\mathbf{q} d\mathcal{A}) \times E \\ & \quad - \int_0^{\mathcal{A}_0} \int_0^L \varepsilon_{m,i} \omega |\boldsymbol{\varphi}|^2 dz d\mathcal{A} \times E, \end{aligned} \quad (\text{B2})$$

where \mathcal{A}_0 is the cross-section area of the domain, over which the surface integration is performed. Simplifying

this expression, one obtains a simple decay law

$$\frac{d}{dt}E = - \underbrace{(\kappa_{\text{tr}} + \kappa_{\text{abs}})}_{\kappa} E, \quad (\text{B3})$$

in which the particular contributions to the total decay rate κ consist of a transmission (Fresnel) term

$$\kappa_{\text{tr}} = \frac{c}{2} \frac{\sqrt{\varepsilon_m(0)}|\varphi(0)|^2 + \sqrt{\varepsilon_m(L)}|\varphi(L)|^2}{\int_C \varepsilon_m(z)|\varphi(z)|^2 dz} \quad (\text{B4})$$

and an absorption term

$$\kappa_{\text{abs}} = \frac{\omega}{2} \frac{\int_{\text{abs}} \varepsilon_{m,i}(z)|\varphi(z)|^2 dz}{\int_C \varepsilon_m(z)|\varphi(z)|^2 dz}. \quad (\text{B5})$$

By $\varepsilon_m(0)$ and $\varepsilon_m(L)$ we understand the permittivity of a nonabsorbing superstrate and substrate, respectively.

Comparing this result with Eq. (40), one derives the following expression for $\tilde{\kappa}$ in the one-dimensional approximation:

$$\begin{aligned} \tilde{\kappa}(z, \omega) &= \tilde{\kappa}_{\text{tr}}(z, \omega) + \tilde{\kappa}_{\text{abs}}(z, \omega) \\ &= \frac{c}{\sqrt{\varepsilon_m(z, \omega)}} \delta(z - z_{\partial C}) + \omega \frac{\varepsilon_{m,i}(z, \omega)}{\varepsilon_m(z, \omega)}. \end{aligned} \quad (\text{B6})$$

In the following, we focus on the κ_{abs} contribution, because it can be significantly simplified in the case of a single absorbing layer. Spatial dependence of $\varepsilon_{m,i}$ can be taken out of the integral, and we obtain

$$\kappa_{\text{abs}} = \Gamma_{\kappa} \left(\frac{\omega}{2} \right) \frac{\varepsilon_{m,i}}{\varepsilon_m}, \quad (\text{B7})$$

where the following confinement factor is defined: $\Gamma_{\kappa} = \int_{\text{abs}} \varepsilon_m(z)|\varphi(z)|^2 dz / \int_C \varepsilon_m(z)|\varphi(z)|^2 dz$. The derived expression is formally almost identical to approximate formulas, which have been derived for anisotropy rates γ_a and γ_p .

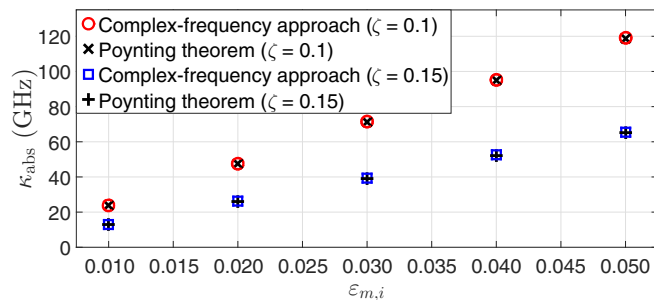


FIG. 13. Calculated cavity-decay-rate contribution coming from internal absorptions κ_{abs} as a function of the imaginary part of the permittivity $\varepsilon_{m,i}$. Results obtained with the robust method based on the matrix formalism are compared with results obtained with the simple analytic expression.

We compare the derived expression with the rigorous and more-powerful method based on the transfer-matrix (or scattering-matrix) formalism. The results, which are in perfect agreement, are shown in Fig. 13.

- [1] F. Meier and B. Zakharchenya, *Optical Orientation* (North Holland, Amsterdam, 1984).
- [2] M. Holub and P. Bhattacharya, Spin-polarized light-emitting diodes and lasers, *J. Phys. D: Appl. Phys.* **40**, R179 (2007).
- [3] N. C. Gerhardt and M. R. Hofmann, Spin-controlled vertical-cavity surface-emitting lasers, *Adv. Opt. Technol.* **2012**, 1 (2012).
- [4] M. Holub, J. Shin, S. Chakrabarti, and P. Bhattacharya, Electrically injected spin-polarized vertical-cavity surface-emitting lasers, *Appl. Phys. Lett.* **87**, 091108 (2005).
- [5] S. Iba, S. Koh, K. Ikeda, and H. Kawaguchi, Room temperature circularly polarized lasing in an optically spin injected vertical-cavity surface-emitting laser with (110) GaAs quantum wells, *Appl. Phys. Lett.* **98**, 081113 (2011).
- [6] J. Rudolph, S. Döhrmann, D. Hägele, M. Oestreich, and W. Stolz, Room-temperature threshold reduction in vertical-cavity surface-emitting lasers by injection of spin-polarized electrons, *Appl. Phys. Lett.* **87**, 241117 (2005).
- [7] M. Holub and B. T. Jonker, Threshold current reduction in spin-polarized lasers: Role of strain and valence-band mixing, *Phys. Rev. B* **83**, 125309 (2011).
- [8] J. Frougier, G. Baili, M. Alouini, I. Sagnes, H. Jaffrès, A. Garnache, C. Deranlot, D. Dolfi, and J.-M. George, Control of light polarization using optically spin-injected vertical external cavity surface emitting lasers, *Appl. Phys. Lett.* **103**, 252402 (2013).
- [9] B. R. Cemlyn, I. D. Henning, M. J. Adams, E. Harbord, R. Oulton, V. Korpjirvi, and M. Guina, Polarization responses of a solitary and optically injected vertical cavity spin laser, *IEEE J. Quantum Electron.* **55**, 1 (2019).
- [10] B. Cemlyn, M. Adams, E. Harbord, N. Li, I. Henning, R. Oulton, V.-M. Korpjirvi, and M. Guina, Near-threshold high spin amplification in a 1300 nm GaInNAs spin laser, *Semicond. Sci. Technol.* **33**, 094005 (2018).
- [11] N. C. Gerhardt, M. Y. Li, H. Jähme, H. Höpfner, T. Ackemann, and M. R. Hofmann, Ultrafast spin-induced polarization oscillations with tunable lifetime in vertical-cavity surface-emitting lasers, *Appl. Phys. Lett.* **99**, 151107 (2011).
- [12] N. Yokota, K. Nisaka, H. Yasaka, and K. Ikeda, Spin polarization modulation for high-speed vertical-cavity surface-emitting lasers, *Appl. Phys. Lett.* **113**, 171102 (2018).
- [13] M. Lindemann, G. Xu, T. Pusch, R. Michalzik, M. Hofmann, I. Žutić, and N. Gerhardt, Ultrafast spin-lasers, *Nature* **568**, 1 (2019).
- [14] R. Safian, G. Ghazi, and N. Mohammadian, Review of photomixing continuous-wave terahertz systems and current application trends in terahertz domain, *Opt. Eng.* **58**, 1 (2019).
- [15] M. Alouini, J. Frougier, A. Joly, G. Baili, D. Dolfi, and J.-M. George, VSPIN: A new model relying on the vectorial description of the laser field for predicting the polarization

- dynamics of spin-injected V(E)CSELS, *Opt. Express* **26**, 6739 (2018).
- [16] J. Frougier, G. Baili, I. Sagnes, D. Dolfi, J.-M. George, and M. Alouini, Accurate measurement of the residual birefringence in VCSEL: Towards understanding of the polarization behavior under spin-polarized pumping, *Opt. Express* **23**, 9573 (2015).
- [17] A. Joly, G. Baili, M. Alouini, J.-M. George, I. Sagnes, G. Pillet, and D. Dolfi, Compensation of the residual linear anisotropy of phase in a vertical-external-cavity-surface-emitting laser for spin injection, *Opt. Lett.* **42**, 651 (2017).
- [18] T. Fördös, K. Postava, H. Jaffrès, and J. Pištora, Matrix approach for modeling of emission from multilayer spin-polarized light-emitting diodes and lasers, *J. Opt.* **16**, 065008 (2014).
- [19] T. Fördös, H. Jaffrès, K. Postava, M. S. Seghilani, A. Garnache, J. Pištora, and H.-J. Drouhin, Eigenmodes of spin vertical-cavity surface-emitting lasers with local linear birefringence and gain dichroism, *Phys. Rev. A* **96**, 043828 (2017).
- [20] H. Benisty, R. Stanley, and M. Mayer, Method of source terms for dipole emission modification in modes of arbitrary planar structures, *J. Opt. Soc. Am. A* **15**, 1192 (1998).
- [21] R. Michalzik, *VCSELS: Fundamentals, Technology and Applications of Vertical-Cavity Surface-Emitting Lasers* (Springer-Verlag, Berlin Heidelberg, 2013).
- [22] T. Fördös, K. Postava, H. Jaffrès, D. Quang To, J. Pištora, and H. J. Drouhin, Mueller matrix ellipsometric study of multilayer spin-VCSEL structures with local optical anisotropy, *Appl. Phys. Lett.* **112**, 221106 (2018).
- [23] S. Balle, Simple analytical approximations for the gain and refractive index spectra in quantum-well lasers, *Phys. Rev. A* **57**, 1304 (1998).
- [24] G. Van der Sande, J. Danckaert, I. Veretennicoff, K. Panajotov, and S. Balle, Analytical approximation for the quantum-well gain and refractive-index spectra of vertical-cavity surface-emitting lasers including the effect of uniaxial planar stress, *Phys. Rev. A* **71**, 063801 (2005).
- [25] P. E. Faria Junior, G. Xu, J. Lee, N. C. Gerhardt, G. M. Sipahi, and I. Žutić, Toward high-frequency operation of spin lasers, *Phys. Rev. B* **92**, 075311 (2015).
- [26] A. Y. Song, A. R. K. Kalapala, W. Zhou, and S. Fan, First-principles simulation of photonic crystal surface-emitting lasers using rigorous coupled wave analysis, *Appl. Phys. Lett.* **113**, 041106 (2018).
- [27] H. E. Türeci, A. D. Stone, and B. Collier, Self-consistent multimode lasing theory for complex or random lasing media, *Phys. Rev. A* **74**, 043822 (2006).
- [28] L. Ge, Y. D. Chong, and A. D. Stone, Steady-state ab initio laser theory: Generalizations and analytic results, *Phys. Rev. A* **82**, 063824 (2010).
- [29] S. Esterhazy, D. Liu, M. Liertz, A. Cerjan, L. Ge, K. G. Makris, A. D. Stone, J. M. Melenk, S. G. Johnson, and S. Rotter, Scalable numerical approach for the steady-state ab initio laser theory, *Phys. Rev. A* **90**, 023816 (2014).
- [30] M. San Miguel, Q. Feng, and J. V. Moloney, Light-polarization dynamics in surface-emitting semiconductor lasers, *Phys. Rev. A* **52**, 1728 (1995).
- [31] J. Martin-Regalado, F. Prati, M. S. Miguel, and N. B. Abraham, Polarization properties of vertical-cavity surface-emitting lasers, *IEEE J. Quantum Electron.* **33**, 765 (1997).
- [32] M. Travagnin, M. P. van Exter, A. K. Jansen van Doorn, and J. P. Woerdman, Role of optical anisotropies in the polarization properties of surface-emitting semiconductor lasers, *Phys. Rev. A* **54**, 1647 (1996).
- [33] M. Travagnin, Linear anisotropies and polarization properties of vertical-cavity surface-emitting semiconductor lasers, *Phys. Rev. A* **56**, 4094 (1997).
- [34] M. Adams, N. Li, B. Cemlyn, H. Susanto, and I. Henning, Algebraic expressions for the polarisation response of spin-VCSELS, *Semicond. Sci. Technol.* **33**, 064002 (2018).
- [35] A. K. Jansen van Doorn, M. P. van Exter, and J. P. Woerdman, Tailoring the birefringence in a vertical-cavity semiconductor laser, *Appl. Phys. Lett.* **69**, 3635 (1996).
- [36] S. Balle, E. Tolkachova, M. S. Miguel, J. R. Tredicce, J. Martín-Regalado, and A. Gahl, Mechanisms of polarization switching in single-transverse-mode vertical-cavity surface-emitting lasers: Thermal shift and nonlinear semiconductor dynamics, *Opt. Lett.* **24**, 1121 (1999).
- [37] D. Burak, J. V. Moloney, and R. Binder, Microscopic theory of polarization properties of optically anisotropic vertical-cavity surface-emitting lasers, *Phys. Rev. A* **61**, 053809 (2000).
- [38] J. Mulet and S. Balle, Spatio-temporal modeling of the optical properties of VCSELS in the presence of polarization effects, *IEEE J. Quantum Electron.* **38**, 291 (2002).
- [39] M. S. Torre, C. Masoller, and P. Mandel, Transverse and polarization effects in index-guided vertical-cavity surface-emitting lasers, *Phys. Rev. A* **74**, 043808 (2006).
- [40] A. Valle, M. Sciamanna, and K. Panajotov, Nonlinear dynamics of the polarization of multitransverse mode vertical-cavity surface-emitting lasers under current modulation, *Phys. Rev. E* **76**, 046206 (2007).
- [41] K. Böhringer and O. Hess, A full-time-domain approach to spatio-temporal dynamics of semiconductor lasers I. Theoretical formulation, *Prog. Quantum. Electron.* **32**, 159 (2008).
- [42] K. Böhringer and O. Hess, A full time-domain approach to spatio-temporal dynamics of semiconductor lasers II. Spatio-temporal dynamics, *Prog. Quantum. Electron.* **32**, 247 (2008).
- [43] M. Vaughan, H. Susanto, I. Henning, and M. Adams, Dynamics of laterally-coupled pairs of spin-VCSELS, *IEEE J. Quantum Electron.* **56**, 1 (2020).
- [44] S. E. Hodges, M. Munroe, J. Cooper, and M. G. Raymer, Multimode laser model with coupled cavities and quantum noise, *J. Opt. Soc. Am. B* **14**, 191 (1997).
- [45] H. Haken, *Light II: Laser Light Dynamics* (North-Holland Publishing Company, Amsterdam, 1985).
- [46] M. Sargent, M. O. Scully, and W. E. Lamb, *Laser Physics* (Addison-Wesley, London, 1974).
- [47] S. V. Zhukovskiy, D. N. Chigrin, and J. Kroha, Bistability and mode interaction in microlasers, *Phys. Rev. A* **79**, 033803 (2009).
- [48] R. Paquet, S. Blin, M. Myara, L. L. Gratiet, M. Sellahi, B. Chomet, G. Beaudoin, I. Sagnes, and A. Garnache, Coherent continuous-wave dual-frequency high-Q external-cavity semiconductor laser for GHz-THz applications, *Opt. Lett.* **41**, 3751 (2016).
- [49] S. Blin, R. Paquet, M. Myara, B. Chomet, L. Le Gratiet, M. Sellahi, G. Beaudoin, I. Sagnes, G. Ducournau, P. Latzel, J. Lampin, and A. Garnache, Coherent and tunable THz

- emission driven by an integrated III–V semiconductor laser, *IEEE J. Sel. Topics Quantum Electron.* **23**, 1 (2017).
- [50] J.-L. Yu, Y.-H. Chen, C.-G. Tang, C. Jiang, and X.-L. Ye, Observation of strong anisotropic forbidden transitions in (001) InGaAs/GaAs single-quantum well by reflectance-difference spectroscopy and its behavior under uniaxial strain, *Nanoscale Res. Lett.* **6**, 210 (2011).
- [51] O. Krebs and P. Voisin, Giant Optical Anisotropy of Semiconductor Heterostructures with No Common Atom and the Quantum-Confined Pockels Effect, *Phys. Rev. Lett.* **77**, 1829 (1996).
- [52] M. S. Park, B. T. Ahn, B.-S. Yoo, H. Y. Chu, H.-H. Park, and C. J. Chang-Hasnain, Polarization control of vertical-cavity surface-emitting lasers by electro-optic birefringence, *Appl. Phys. Lett.* **76**, 813 (2000).
- [53] A. Siegman, *Lasers* (University Science Books, Mill Valley, California, 1986).
- [54] E. L. Ivchenko, A. Y. Kaminski, and U. Rössler, Heavy-light hole mixing at zinc-blende (001) interfaces under normal incidence, *Phys. Rev. B* **54**, 5852 (1996).
- [55] D.-Q. To, Ph.D. thesis, Institut Polytechnique de Paris, cole Polytechnique, 2019.
- [56] P. Yeh, *Optical Waves in Layered Media* (John Wiley and Sons, New York, 1988).
- [57] C. Henry, Theory of the linewidth of semiconductor lasers, *IEEE J. Quantum Electron.* **18**, 259 (1982).
- [58] M. Sargent, W. E. Lamb, and R. L. Fork, Theory of a Zeeman Laser. I, *Phys. Rev.* **164**, 436 (1967).
- [59] M. S. Seghilani, Ph.D. thesis, Université de Montpellier, 2015.
- [60] S. Adachi, Optical dispersion relations for GaP, GaAs, GaSb, InP, InAs, InSb, $\text{Al}_x\text{Ga}_{1-x}\text{As}$, and $\text{In}_{1-x}\text{Ga}_x\text{As}_y\text{P}_{1-y}$, *J. Appl. Phys.* **66**, 6030 (1989).
- [61] M. Drong, T. Fördös, H. Y. Jaffrès, J. Peřina, K. Postava, J. Piřtora, and H.-J. Drouhin, Local and mean-field approaches for modeling semiconductor spin-lasers, *J. Opt.* **22**, 055001 (2020).
- [62] T. Henn, L. Czornomaz, and G. Salis, Characterization of spin-orbit fields in InGaAs quantum wells, *Appl. Phys. Lett.* **109**, 152104 (2016).
- [63] T. C. Damen, L. Viņa, J. E. Cunningham, J. Shah, and L. J. Sham, Subpicosecond Spin Relaxation Dynamics of Excitons and Free Carriers in GaAs Quantum Wells, *Phys. Rev. Lett.* **67**, 3432 (1991).
- [64] E. L. Blansett, M. G. Raymer, G. Khitrova, H. M. Gibbs, D. K. Serkland, A. A. Allerman, and K. M. Geib, Ultrafast polarization dynamics and noise in pulsed vertical-cavity surface-emitting lasers, *Opt. Express* **9**, 312 (2001).
- [65] T. Pusch, S. Scherbl, M. Lindemann, N. C. Gerhardt, M. R. Hofmann, and R. Michalzik, in *Semiconductor Lasers and Laser Dynamics VIII*, edited by K. Panajotov, M. Sciamanna, and R. Michalzik, International Society for Optics and Photonics (SPIE, Strasbourg, 2018), Vol. 10682, p. 120.
- [66] T. Pusch, P. Debernardi, M. Lindemann, F. Erb, N. C. Gerhardt, M. R. Hofmann, and R. Michalzik, Vertical-cavity surface-emitting laser with integrated surface grating for high birefringence splitting, *Electron. Lett.* **55**, 1055 (2019).
- [67] T. Fördös, E. Clarke, P. Patil, R. J. Airey, N. Babazadeh, B. Cemlyn, M. Adams, I. Henning, and J. Heffernan, in *2019 24th Microoptics Conference (MOC)* (IEEE, Toyama, Japan, 2019), p. 306.
- [68] K. Hirose, Y. Liang, Y. Kurosaka, A. Watanabe, T. Sugiyama, and S. Noda, Watt-class high-power, high-beam-quality photonic-crystal lasers, *Nat. Photonics* **8**, 406 (2014).
- [69] K. J. Reilly, A. Kalapala, S. Yeom, S. J. Addamane, E. Renteria, W. Zhou, and G. Balakrishnan, Epitaxial regrowth and hole shape engineering for photonic crystal surface emitting lasers (PCSEs), *J. Cryst. Growth* **535**, 125531 (2020).
- [70] V. Jayaraman, M. Mehta, A. W. Jackson, S. Wu, Y. Okuno, J. Piprek, and J. E. Bowers, High-power 1320-nm wafer-bonded VCSELs with tunnel junctions, *IEEE Photon. Technol. Lett.* **15**, 1495 (2003).
- [71] S. Tang, B. Zhu, M. Jia, Q. He, S. Sun, Y. Mei, and L. Zhou, Effective-medium theory for one-dimensional gratings, *Phys. Rev. B* **91**, 174201 (2015).
- [72] M. Foldyna, R. Ossikovski, A. D. Martino, B. Drevillon, K. Postava, D. Ciprian, J. Piřtora, and K. Watanabe, Effective medium approximation of anisotropic lamellar nanogratings based on Fourier factorization, *Opt. Express* **14**, 3114 (2006).
- [73] N. Haghghi, G. Larisch, R. Rosales, M. Zorn, and J. A. Lott, in *2018 IEEE International Semiconductor Laser Conference (ISLC)* (IEEE, Santa Fe, New Mexico, 2018), p. 1.
- [74] I. Žutić, G. Xu, M. Lindemann, P. E. Faria Junior, J. Lee, V. Labinac, K. Stojřić, G. M. Sipahi, M. R. Hofmann, and N. C. Gerhardt, Spin-lasers: Spintronics beyond magnetoresistance, *Solid State Commun.* **316317**, 113949 (2020).
- [75] K. Postava, T. Fördös, H. Jaffrès, L. Halagačka, H. J. Drouhin, and J. Piřtora, Modeling of anisotropic grating structures with active dipole layers, *Proc. SPIE, Integrated Optics: Phys. Simulations II* 9516, 153 (2015).
- [76] T. Harayama, S. Sunada, and K. S. Ikeda, Theory of two-dimensional microcavity lasers, *Phys. Rev. A* **72**, 013803 (2005).
- [77] R. P. Feynman, R. B. Leighton, and M. Sands, *The Feynman Lectures on Physics* (Addison-Wesley, Reading, Massachusetts, 1966), Vol. II.